From hypersonic to low Mach flows using multi-point numerical methods

Alessia Del Grosso
alessia.del-grosso@inria.fr

Joint work with
Agnes Chan, **Gérard Gallice**, **Raphaël Loubère**, **Pierre-Henri Maire**

CEA Cesta & Institute of Mathematics of Bordeaux & INRIA

28 November 2023

Context & Motivations[1]

Multi-dimensional hyperbolic system of balance laws

$$\partial_t \mathbf{U} + \nabla \cdot \mathbb{F}(\mathbf{U}) = \mathbf{S}(\mathbf{U}),$$

- $\mathbf{U}$ vector of unknowns;
- $\mathbb{F}(\mathbf{U})$ physical flux;
- $\mathbf{S}(\mathbf{U})$ source term.

[1] [Lax (1973), Toro (2009), LeFloch (1988), Audusse et al. (2004), Gallice et al. (2022)]

Context & Motivations[1]

Multi-dimensional hyperbolic system of balance laws

$$\partial_t \mathbf{U} + \nabla \cdot \mathbb{F}(\mathbf{U}) = \mathbf{S}(\mathbf{U}),$$

- $\mathbf{U}$ vector of unknowns;
- $\mathbb{F}(\mathbf{U})$ physical flux;
- $\mathbf{S}(\mathbf{U})$ source term.

Objectif: obtain robust bullet-proof numerical scheme.

[1] [Lax (1973), Toro (2009), LeFloch (1988), Audusse et al. (2004), Gallice et al. (2022)]

Context & Motivations[1]

Multi-dimensional hyperbolic system of balance laws

$$\partial_t \mathbf{U} + \nabla \cdot \mathbb{F}(\mathbf{U}) = \mathbf{S}(\mathbf{U}),$$

- $\mathbf{U}$ vector of unknowns;
- $\mathbb{F}(\mathbf{U})$ physical flux;
- $\mathbf{S}(\mathbf{U})$ source term.

Objectif: obtain robust bullet-proof numerical scheme.

Which properties should the scheme satisfy?

[1] [Lax (1973), Toro (2009), LeFloch (1988), Audusse et al. (2004), Gallice et al. (2022)]

Context & Motivations[1]

Multi-dimensional hyperbolic system of balance laws

$$\partial_t \mathbf{U} + \nabla \cdot \mathbb{F}(\mathbf{U}) = \mathbf{S}(\mathbf{U}),$$

- $\mathbf{U}$ vector of unknowns;
- $\mathbb{F}(\mathbf{U})$ physical flux;
- $\mathbf{S}(\mathbf{U})$ source term.

Objectif: obtain robust bullet-proof numerical scheme.

Which properties should the scheme satisfy?

- Conservation/consistency property
- Domain-preserving (positivity, entropy..)
- Well-balanced property: preservation of stationary solutions

[1] [Lax (1973), Toro (2009), LeFloch (1988), Audusse et al. (2004), Gallice et al. (2022)]

Context & Motivations[1]

Multi-dimensional hyperbolic system of balance laws

$$\partial_t \mathbf{U} + \nabla \cdot \mathbb{F}(\mathbf{U}) = \mathbf{S}(\mathbf{U}),$$

- $\mathbf{U}$ vector of unknowns;
- $\mathbb{F}(\mathbf{U})$ physical flux;
- $\mathbf{S}(\mathbf{U})$ source term.

Objectif: obtain robust bullet-proof numerical scheme.

Which properties should the scheme satisfy?

- Conservation/consistency property
- Domain-preserving (positivity, entropy..)
- Well-balanced property: preservation of stationary solutions
- 2D - 3D: Multi-dimensional-aware scheme

[1] [Lax (1973), Toro (2009), LeFloch (1988), Audusse et al. (2004), Gallice et al. (2022)]

Multi-dimensional finite volume method

Classical scheme

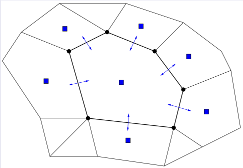

- Dimensional flux-splitting

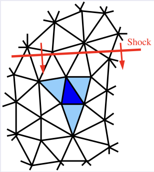

Classical scheme

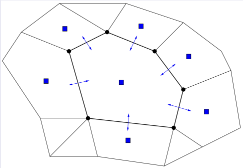

- Dimensional flux-splitting
- Information delay

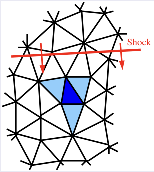

Multi-dimensional finite volume method

Classical scheme

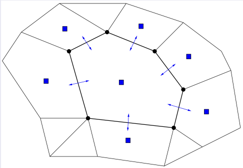

- Dimensional flux-splitting
- Information delay
- Instabilities may arise
- Lost of multi-dimensional properties

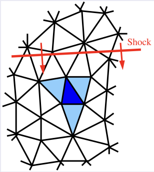

Multi-dimensional finite volume method

Classical scheme

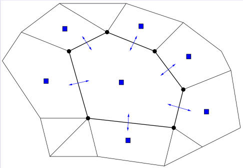

- Dimensional flux-splitting
- Information delay
- Instabilities may arise
- Lost of multi-dimensional properties

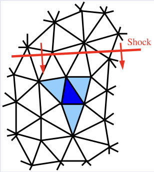

Multi-dimensional-aware scheme

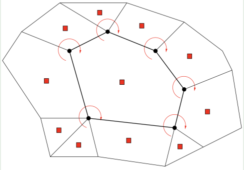

- Consider all cells around
- Information in time

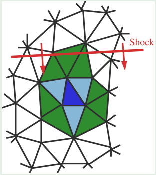

Multi-dimensional finite volume method

Classical scheme

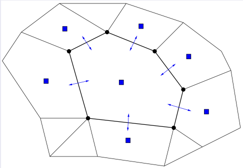

- Dimensional flux-splitting
- Information delay
- Instabilities may arise
- Lost of multi-dimensional properties

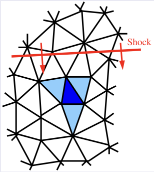

Multi-dimensional-aware scheme

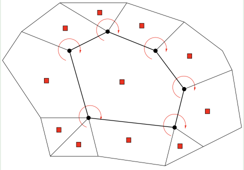

- Consider all cells around
- Information in time

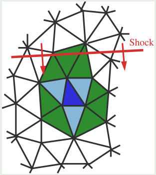

How to consider the entire stencil?

Multi-dimensional finite volume method

Classical scheme

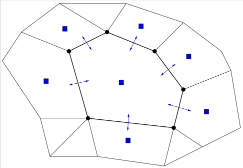

- Dimensional flux-splitting
- Information delay
- Instabilities may arise
- Lost of multi-dimensional properties

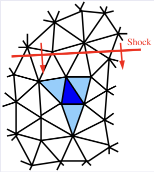

Multi-dimensional-aware scheme

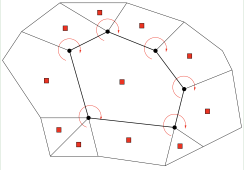

- Consider all cells around
- Information in time

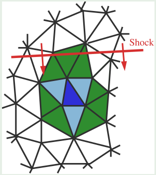

How to consider the entire stencil?

Idea: let us be inspired by the **Lagrangian** world

Eulerian coordinates

Observe the flow from a fixed window

Context & Motivations

Eulerian coordinates

Observe the flow from a fixed window

Lagrangian coordinates

- Move and deform with the flow

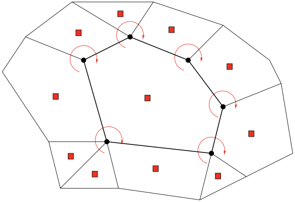

Eulerian coordinates

Observe the flow from a fixed window

Lagrangian coordinates

- Move and deform with the flow
- The mesh moves

Eulerian coordinates

Observe the flow from a fixed window

Lagrangian coordinates

- Move and deform with the flow
- The mesh moves
  $\rightarrow$ **Nodal velocity $\mathbf{u}_p$** (p node) to move the mesh in a compatible manner

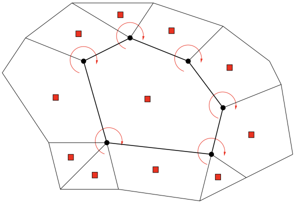

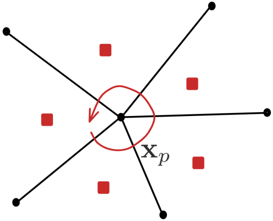

Eulerian coordinates

Observe the flow from a fixed window

Lagrangian coordinates

- Move and deform with the flow
- The mesh moves
  $\rightarrow$ **Nodal velocity $\mathbf{u}_p$** (p node) to move the mesh in a compatible manner
- Concept of **nodal solver** to obtain a nodal parameter

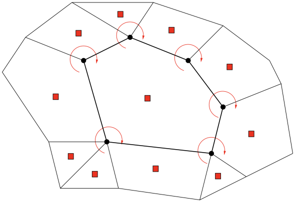

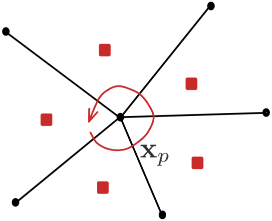

Context & Motivations

Eulerian coordinates

Observe the flow from a fixed window

Lagrangian coordinates

- Move and deform with the flow
- The mesh moves
  $\rightarrow$ **Nodal velocity** $\mathbf{u}_p$ (p node) to move the mesh in a compatible manner
- Concept of **nodal solver** to obtain a nodal parameter
- The flux will depend on the nodal parameter $\mathbf{u}_p$

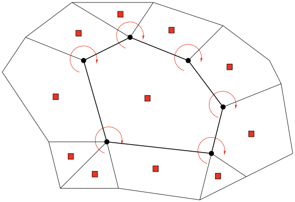

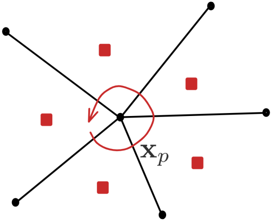

Context & Motivations

Eulerian coordinates

Observe the flow from a fixed window

Lagrangian coordinates

- Move and deform with the flow
- The mesh moves
  $\rightarrow$ **Nodal velocity $\mathbf{u}_p$** (p node) to move the mesh in a compatible manner
- Concept of **nodal solver** to obtain a nodal parameter
- The flux will depend on the nodal parameter $\mathbf{u}_p$

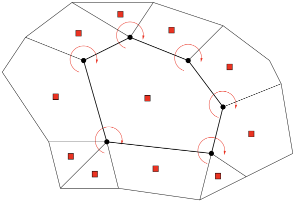

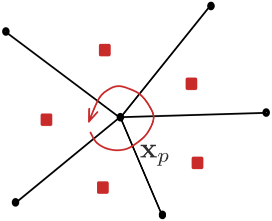

Reference

G. Gallice, A. Chan, R. Loubère, P.-H. Maire.
Entropy Stable and Positivity Preserving Godunov-Type Schemes for Multidimensional Hyperbolic Systems on Unstructured Grid. Journal of Computational Physics, 2022.

Outline

1. Introduction
2. Multi-point scheme for shallow water equations in supersonic flows
   $\rightarrow$ Collaboration with Manuel J. Castro
3. The Carbuncle phenomenon and stability analysis
4. Multi-point scheme for low-Mach flows $\rightarrow$ To be presented in the future

1. Introduction
2. Multi-point scheme for shallow water equations in supersonic flows
   $\rightarrow$ Collaboration with Manuel J. Castro
3. The Carbuncle phenomenon and stability analysis
4. Multi-point scheme for low-Mach flows $\rightarrow$ To be presented in the future

System of Balance Laws: Shallow Water Equations

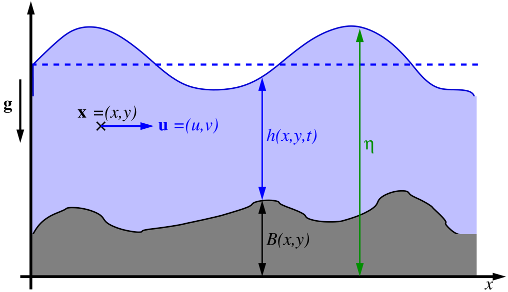

- $h(x, y, t) > 0$ water depth
- $\mathbf{u}(x, y, t)$ averaged velocity of water
- $B(x, y)$ bed elevation
- $\eta = h + B$ free surface elevation

Shallow Water Equations[2]

$$\partial_t \mathbf{U} + \partial_x \mathbf{F}_1(\mathbf{U}) + \partial_y \mathbf{F}_2(\mathbf{U}) = \mathbf{S}(\mathbf{U})$$

$$\begin{cases} \partial_t h + \partial_x(hu) + \partial_y(hv) = 0 \\ \partial_t(hu) + \partial_x(hu^2 + p) + \partial_y(huv) = -gh\partial_x B \\ \partial_t(hu) + \partial_x(huv) + \partial_y(hv^2 + p) = -gh\partial_y B \end{cases}$$

[2] [Vreugdenhil (1994), Temam (2001), Audusse et al. (2004)]

Shallow Water Equations[2]

$$\partial_t \mathbf{U} + \partial_x \mathbf{F}_1(\mathbf{U}) + \partial_y \mathbf{F}_2(\mathbf{U}) = \mathbf{S}(\mathbf{U})$$

$$\begin{cases} \partial_t h + \partial_x(hu) + \partial_y(hv) = 0 \\ \partial_t(hu) + \partial_x(hu^2 + p) + \partial_y(huv) = -gh\partial_x B \\ \partial_t(hu) + \partial_x(huv) + \partial_y(hv^2 + p) = -gh\partial_y B \end{cases}$$

- $p = gh^2/2$ pressure with g gravitational acceleration;

[2] [Vreugdenhil (1994), Temam (2001), Audusse et al. (2004)]

Shallow Water Equations[2]

$$\partial_t \mathbf{U} + \partial_x \mathbf{F}_1(\mathbf{U}) + \partial_y \mathbf{F}_2(\mathbf{U}) = \mathbf{S}(\mathbf{U})$$

$$\begin{cases} \partial_t h + \partial_x(hu) + \partial_y(hv) = 0 \\ \partial_t(hu) + \partial_x(hu^2 + p) + \partial_y(huv) = -gh\partial_x B \\ \partial_t(hu) + \partial_x(huv) + \partial_y(hv^2 + p) = -gh\partial_y B \end{cases}$$

- $p = gh^2/2$ pressure with g gravitational acceleration;
- **Eigenvalues**: given $\mathbf{e} = (e_x, e_y)$, $\mathbf{u} = (u, v)^t$, $a = \sqrt{gh}$,

$$\lambda^- = \mathbf{u} \cdot \mathbf{e} - a, \quad \lambda^- = \mathbf{u} \cdot \mathbf{e}, \quad \lambda^- = \mathbf{u} \cdot \mathbf{e} + a.$$

[2] [Vreugdenhil (1994), Temam (2001), Audusse et al. (2004)]

Shallow Water Equations[2]

$$\partial_t \mathbf{U} + \partial_x \mathbf{F}_1(\mathbf{U}) + \partial_y \mathbf{F}_2(\mathbf{U}) = \mathbf{S}(\mathbf{U})$$

$$\begin{cases} \partial_t h + \partial_x(hu) + \partial_y(hv) = 0 \\ \partial_t(hu) + \partial_x(hu^2 + p) + \partial_y(huv) = -gh\partial_x B \\ \partial_t(hu) + \partial_x(huv) + \partial_y(hv^2 + p) = -gh\partial_y B \end{cases}$$

- $p = gh^2/2$ pressure with g gravitational acceleration;
- **Eigenvalues**: given $\mathbf{e} = (e_x, e_y)$, $\mathbf{u} = (u, v)^t$, $a = \sqrt{gh}$,

$$\lambda^- = \mathbf{u} \cdot \mathbf{e} - a, \quad \lambda^- = \mathbf{u} \cdot \mathbf{e}, \quad \lambda^- = \mathbf{u} \cdot \mathbf{e} + a.$$

- **Entropy** inequality:

$$\partial_t(hE) + \partial_x(uhE + pu) + \partial_y(vhE + pv) \leq -gh\left(u\partial_x B + v\partial_y B\right).$$

[2] [Vreugdenhil (1994), Temam (2001), Audusse et al. (2004)]

Shallow Water Equations[2]

$$\partial_t \mathbf{U} + \partial_x \mathbf{F}_1(\mathbf{U}) + \partial_y \mathbf{F}_2(\mathbf{U}) = \mathbf{S}(\mathbf{U})$$

$$\begin{cases} \partial_t h + \partial_x(hu) + \partial_y(hv) = 0 \\ \partial_t(hu) + \partial_x(hu^2 + p) + \partial_y(huv) = -gh\partial_x B \\ \partial_t(hu) + \partial_x(huv) + \partial_y(hv^2 + p) = -gh\partial_y B \end{cases}$$

- $p = gh^2/2$ pressure with g gravitational acceleration;
- **Eigenvalues**: given $\mathbf{e} = (e_x, e_y)$, $\mathbf{u} = (u, v)^t$, $a = \sqrt{gh}$,

$$\lambda^- = \mathbf{u}\cdot\mathbf{e} - a, \quad \lambda^- = \mathbf{u}\cdot\mathbf{e}, \quad \lambda^- = \mathbf{u}\cdot\mathbf{e} + a.$$

- **Entropy** inequality:

$$\partial_t(hE) + \partial_x(uhE + pu) + \partial_y(vhE + pv) \leq -gh\left(u\partial_x B + v\partial_y B\right).$$

- Stationary solutions: "**lake at rest**" steady state,

$$(u, v) = (0, 0) \quad \text{and} \quad h + B = \text{constant}.$$

[2] [Vreugdenhil (1994), Temam (2001), Audusse et al. (2004)]

Normal $\mathbf{n}$ and tangential $\mathbf{t}$ direction: $u_{\mathbf{n}} = \mathbf{u} \cdot \mathbf{n}$ and $u_{\mathbf{t}} = \mathbf{u} \cdot \mathbf{t}$, with $\mathbf{u} = u_{\mathbf{n}}\mathbf{n} + u_{\mathbf{t}}\mathbf{t}$.

[3] [Gallice et al. (2022), Chan et al. (2021)]

Lagrangian vs Eulerian Coordinates (Normal Direction)[3]

Normal $\mathbf{n}$ and tangential $\mathbf{t}$ direction: $u_\mathbf{n} = \mathbf{u} \cdot \mathbf{n}$ and $u_\mathbf{t} = \mathbf{u} \cdot \mathbf{t}$, with $\mathbf{u} = u_\mathbf{n}\mathbf{n} + u_\mathbf{t}\mathbf{t}$.

Eulerian coordinates: observe the flow from a fixed window

$$\frac{\partial \mathbf{U}_\mathbf{n}}{\partial t} + \frac{\partial \mathbf{F}_\mathbf{n}(\mathbf{U})}{\partial x_\mathbf{n}} = \mathbf{S}_\mathbf{n}(\mathbf{U}),$$

$$\mathbf{U}_\mathbf{n} = \begin{pmatrix} 1 \\ h \\ hu_\mathbf{n} \\ hu_\mathbf{t} \end{pmatrix}, \qquad \mathbf{F}_\mathbf{n} = \begin{pmatrix} 0 \\ hu_\mathbf{n} \\ hu_\mathbf{n}^2 + p(h) \\ hu_\mathbf{n}\, u_\mathbf{t} \end{pmatrix}, \qquad \mathbf{S}_\mathbf{n} = \begin{pmatrix} 0 \\ 0 \\ -gh(\nabla B)_\mathbf{n} \\ 0 \end{pmatrix}.$$

[3] [Gallice et al. (2022), Chan et al. (2021)]

Lagrangian vs Eulerian Coordinates (Normal Direction)[3]

Normal $\mathbf{n}$ and tangential $\mathbf{t}$ direction: $u_\mathbf{n} = \mathbf{u} \cdot \mathbf{n}$ and $u_\mathbf{t} = \mathbf{u} \cdot \mathbf{t}$, with $\mathbf{u} = u_\mathbf{n}\mathbf{n} + u_\mathbf{t}\mathbf{t}$.

Eulerian coordinates: observe the flow from a fixed window

$$\frac{\partial \mathbf{U_n}}{\partial t} + \frac{\partial \mathbf{F_n}(\mathbf{U})}{\partial x_\mathbf{n}} = \mathbf{S_n}(\mathbf{U}),$$

$$\mathbf{U_n} = \begin{pmatrix} 1 \\ h \\ hu_\mathbf{n} \\ hu_\mathbf{t} \end{pmatrix}, \qquad \mathbf{F_n} = \begin{pmatrix} 0 \\ hu_\mathbf{n} \\ hu_\mathbf{n}^2 + p(h) \\ hu_\mathbf{n} u_\mathbf{t} \end{pmatrix}, \qquad \mathbf{S_n} = \begin{pmatrix} 0 \\ 0 \\ -gh(\nabla B)_\mathbf{n} \\ 0 \end{pmatrix}.$$

Lagrangian coordinates: move and deform with the flow

[3] [Gallice et al. (2022), Chan et al. (2021)]

Lagrangian vs Eulerian Coordinates (Normal Direction)[3]

Normal $\mathbf{n}$ and tangential $\mathbf{t}$ direction: $u_\mathbf{n} = \mathbf{u} \cdot \mathbf{n}$ and $u_\mathbf{t} = \mathbf{u} \cdot \mathbf{t}$, with $\mathbf{u} = u_\mathbf{n}\mathbf{n} + u_\mathbf{t}\mathbf{t}$.

Eulerian coordinates: observe the flow from a fixed window

$$\frac{\partial \mathbf{U}_\mathbf{n}}{\partial t} + \frac{\partial \mathbf{F}_\mathbf{n}(\mathbf{U})}{\partial x_\mathbf{n}} = \mathbf{S}_\mathbf{n}(\mathbf{U}),$$

$$\mathbf{U}_\mathbf{n} = \begin{pmatrix} 1 \\ h \\ hu_\mathbf{n} \\ hu_\mathbf{t} \end{pmatrix}, \qquad \mathbf{F}_\mathbf{n} = \begin{pmatrix} 0 \\ hu_\mathbf{n} \\ hu_\mathbf{n}^2 + p(h) \\ hu_\mathbf{n} u_\mathbf{t} \end{pmatrix}, \qquad \mathbf{S}_\mathbf{n} = \begin{pmatrix} 0 \\ 0 \\ -gh(\nabla B)_\mathbf{n} \\ 0 \end{pmatrix}.$$

Lagrangian coordinates: move and deform with the flow

$$\frac{\partial \mathbf{V}_\mathbf{n}}{\partial t} + \frac{\partial \mathbf{G}_\mathbf{n}(\mathbf{V})}{\partial m} = \mathbf{P}_\mathbf{n}(\mathbf{V}_\mathbf{n}),$$

$$\mathbf{V}_\mathbf{n} = \tau \mathbf{U}_\mathbf{n} = \begin{pmatrix} \tau \\ 1 \\ u_\mathbf{n} \\ u_\mathbf{t} \end{pmatrix}, \qquad \mathbf{G}_\mathbf{n} = \mathbf{F}_\mathbf{n} - u_\mathbf{n}\mathbf{U}_\mathbf{n} = \begin{pmatrix} -u_\mathbf{n} \\ 0 \\ p \\ 0 \end{pmatrix}, \qquad \mathbf{P}_\mathbf{n}(\mathbf{V}_\mathbf{n}) = \begin{pmatrix} 0 \\ 0 \\ -gh\partial_m B \\ 0 \end{pmatrix},$$

V volume, $m = hV$ mass variable, $\tau = 1/h$.

[3] [Gallice et al. (2022), Chan et al. (2021)]

Lagrangian vs Eulerian Coordinates (Normal Direction)[3]

Normal $\mathbf{n}$ and tangential $\mathbf{t}$ direction: $u_\mathbf{n} = \mathbf{u}\cdot\mathbf{n}$ and $u_\mathbf{t} = \mathbf{u}\cdot\mathbf{t}$, with $\mathbf{u} = u_\mathbf{n}\mathbf{n} + u_\mathbf{t}\mathbf{t}$.

Eulerian coordinates: observe the flow from a fixed window

$$\frac{\partial \mathbf{U}_\mathbf{n}}{\partial t} + \frac{\partial \mathbf{F}_\mathbf{n}(\mathbf{U})}{\partial x_\mathbf{n}} = \mathbf{S}_\mathbf{n}(\mathbf{U}),$$

$$\mathbf{U}_\mathbf{n} = \begin{pmatrix} 1 \\ h \\ hu_\mathbf{n} \\ hu_\mathbf{t} \end{pmatrix}, \qquad \mathbf{F}_\mathbf{n} = \begin{pmatrix} 0 \\ hu_\mathbf{n} \\ hu_\mathbf{n}^2 + p(h) \\ hu_\mathbf{n} u_\mathbf{t} \end{pmatrix}, \qquad \mathbf{S}_\mathbf{n} = \begin{pmatrix} 0 \\ 0 \\ -gh(\nabla B)_\mathbf{n} \\ 0 \end{pmatrix}.$$

Lagrangian coordinates: move and deform with the flow

$$\frac{\partial \mathbf{V}_\mathbf{n}}{\partial t} + \frac{\partial \mathbf{G}_\mathbf{n}(\mathbf{V})}{\partial m} = \mathbf{P}_\mathbf{n}(\mathbf{V}_\mathbf{n}),$$

$$\mathbf{V}_\mathbf{n} = \tau \mathbf{U}_\mathbf{n} = \begin{pmatrix} \tau \\ 1 \\ u_\mathbf{n} \\ u_\mathbf{t} \end{pmatrix}, \qquad \mathbf{G}_\mathbf{n} = \mathbf{F}_\mathbf{n} - u_\mathbf{n}\mathbf{U}_\mathbf{n} = \begin{pmatrix} -u_\mathbf{n} \\ 0 \\ p \\ 0 \end{pmatrix}, \qquad \mathbf{P}_\mathbf{n}(\mathbf{V}_\mathbf{n}) = \begin{pmatrix} 0 \\ 0 \\ -gh\partial_m B \\ 0 \end{pmatrix},$$

V volume, $m = hV$ mass variable, $\tau = 1/h$.

[3] [Gallice et al. (2022), Chan et al. (2021)]

Notations

- c cell index with ω_c polygonal cell
- $\mathbf{x}_p$ vector position of node p
- p^- (p^+) previous (next) point with respect to p
- $\mathcal{P}(c)$ set of vertices (points) of ω_c
- f face, l_{pcf} measure of the subface f
- $\mathbf{n}_{pcf} = (n_x, n_y)_{pcf}$ unit outward normal of the subface
- ω_{pc} quadrangle formed by joining the cell centroid, $\mathbf{x}_c$, to the midpoints of $[\mathbf{x}_{p^-}, \mathbf{x}_p]$, $[\mathbf{x}_p, \mathbf{x}_{p^+}]$ and to $\mathbf{x}_p$
- $\mathcal{SF}(pc)$ set of subfaces for $p \in \mathcal{P}(c)$

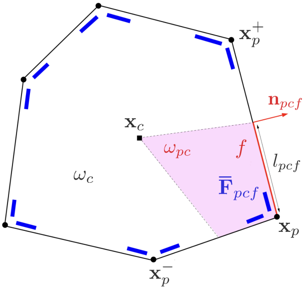

Figure: Geometrical entities attached to the polygonal cell ω_c.

Notations

- c cell index with ω_c polygonal cell
- $\mathbf{x}_p$ vector position of node p
- p^- (p^+) previous (next) point with respect to p
- $\mathcal{P}(c)$ set of vertices (points) of ω_c
- f face, l_{pcf} measure of the subface f
- $\mathbf{n}_{pcf} = (n_x, n_y)_{pcf}$ unit outward normal of the subface
- ω_{pc} quadrangle formed by joining the cell centroid, $\mathbf{x}_c$, to the midpoints of $[\mathbf{x}_{p^-}, \mathbf{x}_p]$, $[\mathbf{x}_p, \mathbf{x}_{p^+}]$ and to $\mathbf{x}_p$
- $\mathcal{SF}(pc)$ set of subfaces for $p \in \mathcal{P}(c)$

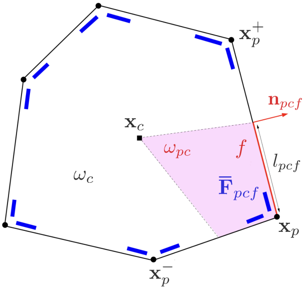

Figure: Geometrical entities attached to the polygonal cell ω_c.

Notations

- c cell index with ω_c polygonal cell
- $\mathbf{x}_p$ vector position of node p
- p^- (p^+) previous (next) point with respect to p
- $\mathcal{P}(c)$ set of vertices (points) of ω_c
- f face, l_{pcf} measure of the subface f
- $\mathbf{n}_{pcf} = (n_x, n_y)_{pcf}$ unit outward normal of the subface
- ω_{pc} quadrangle formed by joining the cell centroid, $\mathbf{x}_c$, to the midpoints of $[\mathbf{x}_{p^-}, \mathbf{x}_p]$, $[\mathbf{x}_p, \mathbf{x}_{p^+}]$ and to $\mathbf{x}_p$
- $\mathcal{SF}(pc)$ set of subfaces for $p \in \mathcal{P}(c)$

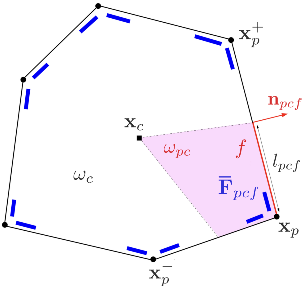

Figure: Geometrical entities attached to the polygonal cell ω_c.

What about the flux $\widetilde{\mathbf{F}}_{pcf}$ which should depend on the nodal velocity $\mathbf{u}_p$?

Face Flux VS Subface Flux

Face flux for classical two-point schemes

$$\widetilde{\mathbf{F}}_{cf} = \widetilde{\mathbf{F}}_{cf}(\mathbf{U}_c^n, \mathbf{U}_d^n, B_c, B_d, \mathbf{n}_{cf})$$

- Classical **conservation**
  $\rightarrow$ **left flux = -right flux** .

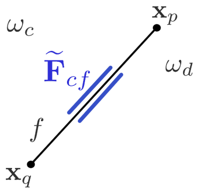

Figure: Two-point scheme

Face Flux VS Subface Flux

Face flux for classical two-point schemes

$$\widetilde{\mathbf{F}}_{cf} = \widetilde{\mathbf{F}}_{cf}(\mathbf{U}_c^n, \mathbf{U}_d^n, B_c, B_d, \mathbf{n}_{cf})$$

- Classical **conservation**
  $\rightarrow$ **left flux = -right flux** .

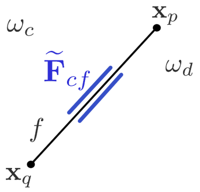

Figure: Two-point scheme

Subface flux for multi-point scheme

$$\widetilde{\mathbf{F}}_{pcf} = \widetilde{\mathbf{F}}_{pcf}(\mathbf{U}_c^n, \mathbf{U}_d^n, B_c, B_d, \mathbf{n}_{pcf}, \mathbf{u}_p)$$

- $\mathbf{u}_p$ **nodal parameter.**

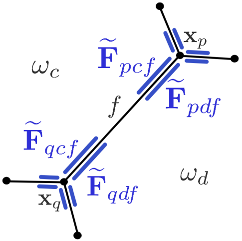

Figure: Multi-point scheme

Face Flux VS Subface Flux

Face flux for classical two-point schemes

$$\widetilde{\mathbf{F}}_{cf} = \widetilde{\mathbf{F}}_{cf}(\mathbf{U}_c^n, \mathbf{U}_d^n, B_c, B_d, \mathbf{n}_{cf})$$

- Classical **conservation** $\rightarrow$ **left flux = -right flux** .

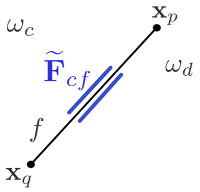

Figure: Two-point scheme

Subface flux for multi-point scheme

$$\widetilde{\mathbf{F}}_{pcf} = \widetilde{\mathbf{F}}_{pcf}(\mathbf{U}_c^n, \mathbf{U}_d^n, B_c, B_d, \mathbf{n}_{pcf}, \mathbf{u}_p)$$

- $\mathbf{u}_p$ **nodal parameter.**
- **Lost of classical conservation.**

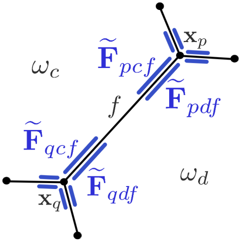

Figure: Multi-point scheme

Face Flux VS Subface Flux

Face flux for classical two-point schemes

$$\widetilde{\mathbf{F}}_{cf} = \widetilde{\mathbf{F}}_{cf}(\mathbf{U}_c^n, \mathbf{U}_d^n, B_c, B_d, \mathbf{n}_{cf})$$

- Classical **conservation**
  $\rightarrow$ **left flux = -right flux** .

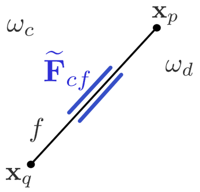

Figure: Two-point scheme

Subface flux for multi-point scheme

$$\widetilde{\mathbf{F}}_{pcf} = \widetilde{\mathbf{F}}_{pcf}(\mathbf{U}_c^n, \mathbf{U}_d^n, B_c, B_d, \mathbf{n}_{pcf}, \mathbf{u}_p)$$

- **$\mathbf{u}_p$ nodal parameter.**
- **Lost of classical conservation.**
- Conservation will be recovered by the nodal solver.

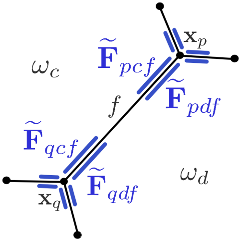

Figure: Multi-point scheme

Subface-based Finite Volume Scheme

Integration in time and space

$$|\omega_c| \mathrm{d}_t \mathbf{U}_c + \int_{\partial \omega_c} \mathbf{F}(\mathbf{U}) \mathbf{n} \, \mathrm{d}s = \int_{\omega_c} \mathbf{S}(\mathbf{U}) \, \mathrm{d}v$$

$$\text{with} \quad \mathbf{U}_c(t) = \frac{1}{|\omega_c|} \int_{\omega_c} \mathbf{U}(\mathbf{x}, t) \, \mathrm{d}v.$$

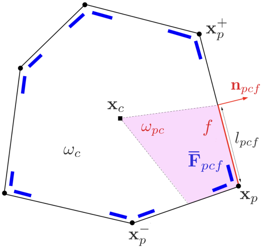

Subface-based Finite Volume Scheme

Integration in time and space

$$|\omega_c| \mathrm{d}_t \mathbf{U}_c + \int_{\partial\omega_c} \mathbf{F}(\mathbf{U})\mathbf{n}\,\mathrm{d}s = \int_{\omega_c} \mathbf{S}(\mathbf{U})\,\mathrm{d}v$$

with $\quad \mathbf{U}_c(t) = \dfrac{1}{|\omega_c|} \displaystyle\int_{\omega_c} \mathbf{U}(\mathbf{x}, t)\,\mathrm{d}v.$

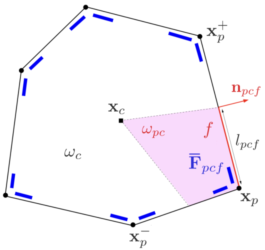

Subface-based finite volume scheme

$$\mathbf{U}_c^{n+1} = \mathbf{U}_c^n - \frac{\Delta t}{|\omega_c|} \sum_{p \in \mathcal{P}(c)} \sum_{f \in \mathcal{SF}(pc)} \left[l_{pcf} \overline{\mathbf{F}}_{pcf} - w_{pcf} \overline{\mathbf{S}}_{pcf} \right]$$

$$= \mathbf{U}_c^n - \frac{\Delta t}{|\omega_c|} \sum_{p \in \mathcal{P}(c)} \sum_{f \in \mathcal{SF}(pc)} l_{pcf} \widetilde{\mathbf{F}}_{pcf}.$$

Subface-based Finite Volume Scheme

Integration in time and space

$$|\omega_c| \mathrm{d}_t \mathbf{U}_c + \int_{\partial\omega_c} \mathbf{F}(\mathbf{U})\mathbf{n}\,\mathrm{d}s = \int_{\omega_c} \mathbf{S}(\mathbf{U})\,\mathrm{d}v$$

$$\text{with} \quad \mathbf{U}_c(t) = \frac{1}{|\omega_c|} \int_{\omega_c} \mathbf{U}(\mathbf{x},t)\,\mathrm{d}v.$$

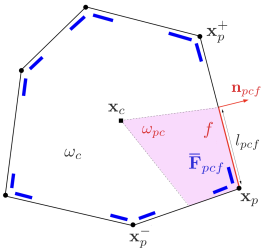

Subface-based finite volume scheme

$$\mathbf{U}_c^{n+1} = \mathbf{U}_c^n - \frac{\Delta t}{|\omega_c|} \sum_{p\in\mathcal{P}(c)} \sum_{f\in\mathcal{SF}(pc)} \left[l_{pcf}\overline{\mathbf{F}}_{pcf} - w_{pcf}\overline{\mathbf{S}}_{pcf} \right]$$

$$= \mathbf{U}_c^n - \frac{\Delta t}{|\omega_c|} \sum_{p\in\mathcal{P}(c)} \sum_{f\in\mathcal{SF}(pc)} l_{pcf}\widetilde{\mathbf{F}}_{pcf}.$$

$$\widetilde{\mathbf{F}}_{\mathbf{n}_{pcf}} = \mathbb{F}(\mathbf{U}_{lf})\mathbf{n}_{pcf} - \int_{-\infty}^{0} \left[\mathbf{W}_{pcf,\mathcal{E}}(\mathbf{U}_{lf}, \mathbf{U}_{rf}, B_{lf}, B_{rf}, \mathbf{n}_{pcf}, \xi, \mathbf{u}_p) - \mathbf{U}_{lf} \right] \mathrm{d}\xi$$

Lagrangian Approximate Riemann solver[4]

Riemann problem (normal direction)

$$\begin{cases} \dfrac{\partial \mathbf{V}_{\mathbf{n}_{pf}}}{\partial t} + \dfrac{\partial [\mathbf{G}_{\mathbf{n}_{pf}}(\mathbf{V})]}{\partial m_{\mathbf{n}_{pf}}} = \mathbf{P}_{\mathbf{n}_{pf}}, \\ \mathbf{V}_{\mathbf{n}_{pf}}(m_{\mathbf{n}_{pf}}, 0) = \begin{cases} \mathbf{V}_{Lf} & \text{if } m_{\mathbf{n}_{pf}} < 0, \\ \mathbf{V}_{Rf} & \text{if } m_{\mathbf{n}_{pf}} \geq 0. \end{cases} \end{cases}$$

[4] [Gallice (2002)]

Lagrangian Approximate Riemann solver[4]

Riemann problem (normal direction)

$$\begin{cases} \dfrac{\partial \mathbf{V}_{\mathbf{n}_{pf}}}{\partial t} + \dfrac{\partial [\mathbf{G}_{\mathbf{n}_{pf}}(\mathbf{V})]}{\partial m_{\mathbf{n}_{pf}}} = \mathbf{P}_{\mathbf{n}_{pf}}, \\ \mathbf{V}_{\mathbf{n}_{pf}}(m_{\mathbf{n}_{pf}}, 0) = \begin{cases} \mathbf{V}_{Lf} & \text{if } m_{\mathbf{n}_{pf}} < 0, \\ \mathbf{V}_{Rf} & \text{if } m_{\mathbf{n}_{pf}} \geq 0. \end{cases} \end{cases}$$

Three **ordered** waves:

$$-\lambda_{Lf} < \lambda_0 = 0 < \lambda_{Rf}.$$

Approximate Riemann solver

$\mathbf{W}_{pf,\mathcal{L}}$ depends on $\mathbf{u}_p$ and it is such that

$$\mathbf{W}_{pf,\mathcal{L}} = \begin{cases} \mathbf{V}_{Lf} & \text{if} \quad \xi < \lambda_{Lf}, \\ \mathbf{V}^{\star}_{Lf} & \text{if} \quad \lambda_{Lf} < \xi \leq 0 \\ \mathbf{V}^{\star}_{Rf} & \text{if} \quad 0 < \xi \leq \lambda_{Rf} \\ \mathbf{V}_{Rf} & \text{if} \quad \lambda_{Rf} \leq \xi. \end{cases}$$

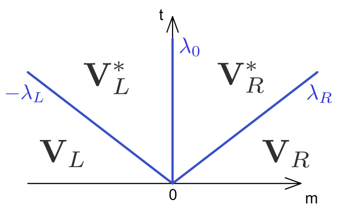

[4] [Gallice (2002)]

Lagrangian Approximate Riemann solver[4]

Riemann problem (normal direction)

$$\begin{cases} \dfrac{\partial \mathbf{V}_{\mathbf{n}_{pf}}}{\partial t} + \dfrac{\partial [\mathbf{G}_{\mathbf{n}_{pf}}(\mathbf{V})]}{\partial m_{\mathbf{n}_{pf}}} = \mathbf{P}_{\mathbf{n}_{pf}}, \\ \mathbf{V}_{\mathbf{n}_{pf}}(m_{\mathbf{n}_{pf}}, 0) = \begin{cases} \mathbf{V}_{Lf} & \text{if } m_{\mathbf{n}_{pf}} < 0, \\ \mathbf{V}_{Rf} & \text{if } m_{\mathbf{n}_{pf}} \geq 0. \end{cases} \end{cases}$$

Three **ordered** waves:

$$-\lambda_{Lf} < \lambda_0 = 0 < \lambda_{Rf}.$$

Rankine-Hugoniot conditions

Across left and right waves:

$$\lambda_{Lf}(\mathbf{V}^{\star}_{Lf} - \mathbf{V}_{Lf}) + \mathbf{G}^{\star}_{\mathbf{n},Lf} - \mathbf{G}_{\mathbf{n},Lf} = 0,$$
$$-\lambda_{Rf}(\mathbf{V}_{Rf} - \mathbf{V}^{\star}_{Rf}) + \mathbf{G}_{\mathbf{n},Rf} - \mathbf{G}^{\star}_{\mathbf{n},Rf} = 0.$$

Approximate Riemann solver

$\mathbf{W}_{pf,\mathcal{L}}$ depends on $\mathbf{u}_p$ and it is such that

$$\mathbf{W}_{pf,\mathcal{L}} = \begin{cases} \mathbf{V}_{Lf} & \text{if} \quad \xi < \lambda_{Lf}, \\ \mathbf{V}^{\star}_{Lf} & \text{if} \quad \lambda_{Lf} < \xi \leq 0 \\ \mathbf{V}^{\star}_{Rf} & \text{if} \quad 0 < \xi \leq \lambda_{Rf} \\ \mathbf{V}_{Rf} & \text{if} \quad \lambda_{Rf} \leq \xi. \end{cases}$$

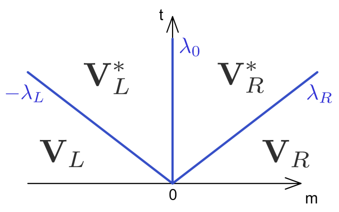

4 [Gallice (2002)]

Node-based Consistency Conditions

What to do across the 0-wave ?

Node-based Consistency Conditions

What to do across the 0-wave ?

- For the mass equation, classical jump condition: $u^{\star}_{\mathbf{n},R} = u^{\star}_{\mathbf{n},L} = u^{\star}_{\mathbf{n}}$.

Node-based Consistency Conditions

What to do across the 0-wave ?

- For the mass equation, classical jump condition: $u^\star_{\mathbf{n},R} = u^\star_{\mathbf{n},L} = u^\star_{\mathbf{n}}$.
- For the other equations, we do not say anything $\Longrightarrow$ $p^\star_R \neq p^\star_L$ in general

Node-based Consistency Conditions

What to do across the 0-wave ?

- For the mass equation, classical jump condition: $u^\star_{\mathbf{n},R} = u^\star_{\mathbf{n},L} = u^\star_{\mathbf{n}}$.
- For the other equations, we do not say anything $\Longrightarrow$ $p^\star_R \neq p^\star_L$ in general
- We are left with only one unknown: $u^\star_{\mathbf{n}}$

Node-based Consistency Conditions

What to do across the 0-wave ?

- For the mass equation, classical jump condition: $u^\star_{\mathbf{n},R} = u^\star_{\mathbf{n},L} = u^\star_{\mathbf{n}}$.
- For the other equations, we do not say anything $\Longrightarrow$ $p^\star_R \neq p^\star_L$ in general
- We are left with only one unknown: $u^\star_{\mathbf{n}}$

Classical **face-based** jump condition

$$\widetilde{\mathbf{G}}^R_{\mathbf{n},pf} - \widetilde{\mathbf{G}}^L_{\mathbf{n},pf} = (\Delta m_{Lf} + \Delta m_{Rf})\mathbf{P}_{\mathbf{n}_{pf}}(\Delta m_{Lf}, \Delta m_{Rf}, \mathbf{V}_{Lf}, \mathbf{V}_{Rf}).$$

If there is no source term, conservation is obtained:

$$\widetilde{\mathbf{G}}^R_{\mathbf{n},pf} - \widetilde{\mathbf{G}}^L_{\mathbf{n},pf} = 0.$$

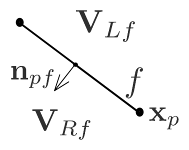

Node-based Consistency Conditions

What to do across the 0-wave ?

- For the mass equation, classical jump condition: $u^\star_{\mathbf{n},R} = u^\star_{\mathbf{n},L} = u^\star_{\mathbf{n}}$.
- For the other equations, we do not say anything $\Longrightarrow$ $p^\star_R \neq p^\star_L$ in general
- We are left with only one unknown: $u^\star_{\mathbf{n}}$

Classical **face-based** consistency conditions

$$\lambda_{Lf}(\mathbf{V}^\star_{Lf} - \mathbf{V}_{Lf}) - \lambda_{Rf}(\mathbf{V}_{Rf} - \mathbf{V}^\star_{Rf})$$

$$+ \left(\mathbb{G}(\mathbf{V}_{Rf}) - \mathbb{G}(\mathbf{V}_{Lf})\right)\mathbf{n}_{pf}$$

$$- (\Delta m_{Lf} + \Delta m_{Rf})\mathbf{P}_{\mathbf{n}_{pf}}(\Delta m_{Lf}, \Delta m_{Rf}, \mathbf{V}_{Lf}, \mathbf{V}_{Rf}, B_{Lf}, B_{Rf}) \quad = \mathbf{0}.$$

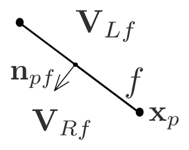

Node-based Consistency Conditions

What to do across the 0-wave ?

- For the mass equation, classical jump condition: $u^\star_{\mathbf{n},R} = u^\star_{\mathbf{n},L} = u^\star_{\mathbf{n}}$.
- For the other equations, we do not say anything $\Longrightarrow$ $p^\star_R \neq p^\star_L$ in general
- We are left with only one unknown: $u^\star_{\mathbf{n}}$

Node-based consistency conditions

$$\sum_{f\in\mathcal{SF}(p)} l_{pf} \Big[\lambda_{Lf}(\mathbf{V}^\star_{Lf} - \mathbf{V}_{Lf}) - \lambda_{Rf}(\mathbf{V}_{Rf} - \mathbf{V}^\star_{Rf}) + (\mathbb{G}(\mathbf{V}_{Rf}) - \mathbb{G}(\mathbf{V}_{Lf}))\,\mathbf{n}_{pf} - (\Delta m_{Lf} + \Delta m_{Rf})\mathbf{P}_{\mathbf{n}_{pf}}(\Delta m_{Lf}, \Delta m_{Rf}, \mathbf{V}_{Lf}, \mathbf{V}_{Rf}, B_{Lf}, B_{Rf}) \Big] = \mathbf{0}.$$

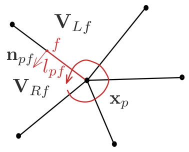

Node-based Consistency Conditions

What to do across the 0-wave ?

- For the mass equation, classical jump condition: $u^\star_{\mathbf{n},R} = u^\star_{\mathbf{n},L} = u^\star_{\mathbf{n}}$.
- For the other equations, we do not say anything $\Longrightarrow$ $p^\star_R \neq p^\star_L$ in general
- We are left with only one unknown: $u^\star_{\mathbf{n}}$

Node-based jump condition

$$\sum_{f\in\mathcal{SF}(p)} l_{pf} \left[\widetilde{\mathbf{G}}^R_{\mathbf{n},pf} - \widetilde{\mathbf{G}}^L_{\mathbf{n},pf} \right]$$

$$= \sum_{f\in\mathcal{SF}(p)} l_{pf} (\Delta m_{Lf} + \Delta m_{Rf}) \mathbf{P}_{\mathbf{n}_{pf}} (\Delta m_{Lf}, \Delta m_{Rf}, \mathbf{V}_{Lf}, \mathbf{V}_{Rf}).$$

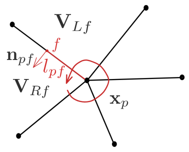

Node-based Consistency Conditions

What to do across the 0-wave ?

- For the mass equation, classical jump condition: $u^\star_{\mathbf{n},R} = u^\star_{\mathbf{n},L} = u^\star_{\mathbf{n}}$.
- For the other equations, we do not say anything $\Longrightarrow$ $p^\star_R \neq p^\star_L$ in general
- We are left with only one unknown: $u^\star_{\mathbf{n}}$

Node-based consistency conditions

$$\sum_{f \in \mathcal{SF}(p)} l_{pf} (p^\star_{Rf} - p^\star_{Lf} + g\overline{h\Delta B}_{LR,f})\mathbf{n}_{pf} = \mathbf{0}.$$

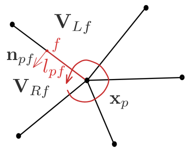

Node-based Consistency Conditions

What to do across the 0-wave ?

- For the mass equation, classical jump condition: $u^\star_{\mathbf{n},R} = u^\star_{\mathbf{n},L} = u^\star_{\mathbf{n}}$.
- For the other equations, we do not say anything $\Longrightarrow$ $p^\star_R \neq p^\star_L$ in general
- We are left with only one unknown: $u^\star_{\mathbf{n}}$

Node-based consistency conditions

$$\sum_{f \in \mathcal{SF}(p)} l_{pf}\left(p^\star_{Rf} - p^\star_{Lf} + g\overline{h\Delta B}_{LR,f}\right)\mathbf{n}_{pf} = \mathbf{0}.$$

with $$\begin{cases} p^\star_L = p_L - \lambda_L(u^\star_{\mathbf{n}} - u_{\mathbf{n},L}) \\ p^\star_R = p_R + \lambda_R(u^\star_{\mathbf{n}} - u_{\mathbf{n},R}) \end{cases}$$

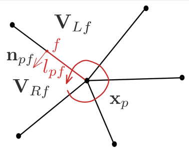

Node-based Consistency Conditions

What to do across the 0-wave ?

- For the mass equation, classical jump condition: $u^\star_{\mathbf{n},R} = u^\star_{\mathbf{n},L} = u^\star_{\mathbf{n}}$.
- For the other equations, we do not say anything $\Longrightarrow$ $p^\star_R \neq p^\star_L$ in general
- We are left with only one unknown: $u^\star_{\mathbf{n}}$

Node-based consistency conditions

$$\sum_{f\in\mathcal{SF}(p)} l_{pf}(\lambda_{L,f}+\lambda_{R,f})(u^\star_{\mathbf{n}_{pf}} - u^{\mathrm{Godv}}_{\mathbf{n}_{pf}})\mathbf{n}_{pf} = \mathbf{0},$$

with $$u^{\mathrm{Godv}}_{\mathbf{n}} = \frac{\lambda_L u_{\mathbf{n},L} + \lambda_R u_{\mathbf{n},R}}{\lambda_L+\lambda_R} - \frac{(p_R - p_L + g\overline{h\Delta B}_{LR})}{\lambda_R+\lambda_L}.$$

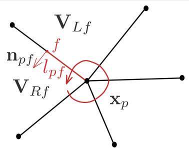

Node-based Consistency Conditions

What to do across the 0-wave ?

- For the mass equation, classical jump condition: $u^\star_{\mathbf{n},R} = u^\star_{\mathbf{n},L} = u^\star_{\mathbf{n}}$.
- For the other equations, we do not say anything $\Longrightarrow$ $p^\star_R \neq p^\star_L$ in general
- We are left with only one unknown: $u^\star_{\mathbf{n}}$

Node-based consistency conditions

$$\sum_{f\in\mathcal{SF}(p)} l_{pf}(\lambda_{L,f} + \lambda_{R,f})(u^\star_{\mathbf{n}_{pf}} - u^{\mathrm{Godv}}_{\mathbf{n}_{pf}})\mathbf{n}_{pf} = \mathbf{0},$$

$$\text{with} \quad u^\star_{\mathbf{n}_{pf}} = \mathbf{u}_p \cdot \mathbf{n}_{pf}.$$

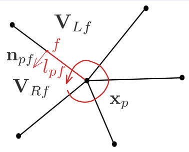

Node-based Consistency Conditions

What to do across the 0-wave ?

- For the mass equation, classical jump condition: $u^{\star}_{\mathbf{n},R} = u^{\star}_{\mathbf{n},L} = u^{\star}_{\mathbf{n}}$.
- For the other equations, we do not say anything $\Longrightarrow$ $p^{\star}_{R} \neq p^{\star}_{L}$ in general
- We are left with only one unknown: $u^{\star}_{\mathbf{n}}$

Node-based consistency conditions

$$\sum_{f \in \mathcal{SF}(p)} l_{pf}(\lambda_{L,f} + \lambda_{R,f})(\mathbf{u}_p \cdot \mathbf{n}_{pf} - u^{\mathrm{Godv}}_{\mathbf{n}_{pf}})\mathbf{n}_{pf} = \mathbf{0}.$$

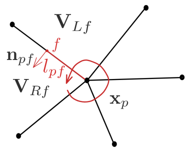

Node-based Consistency Conditions

What to do across the 0-wave ?

- For the mass equation, classical jump condition: $u^\star_{\mathbf{n},R} = u^\star_{\mathbf{n},L} = u^\star_{\mathbf{n}}$.
- For the other equations, we do not say anything $\Longrightarrow$ $p^\star_R \neq p^\star_L$ in general
- We are left with only one unknown: $u^\star_{\mathbf{n}}$

Node-based consistency conditions Nodal solver

$$\mathbb{M}_p \, \mathbf{u}_p = \mathbf{w}_p$$

where $\displaystyle \mathbb{M}_p = \sum_{f \in \mathcal{SF}(p)} l_{pf}(\lambda_{lf} + \lambda_{rf})(\mathbf{n}_{pf} \otimes \mathbf{n}_{pf}),$

and $\displaystyle \mathbf{w}_p = \sum_{f \in \mathcal{SF}(p)} l_{pf}(\lambda_{lf} + \lambda_{rf}) u^{Godv}_{\mathbf{n}_{pf}} \mathbf{n}_{pf}.$

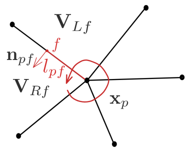

Properties of the approximate Riemann solver

Well-balanced property

If $\mathbf{V}_{Lf}$ and $\mathbf{V}_{Rf}$ verify the steady "lake at rest" solution, we ask for

$$\mathbf{V}^{\star}_{Lf} = \mathbf{V}_{Lf} \quad \text{and} \quad \mathbf{V}^{\star}_{Rf} = \mathbf{V}_{Rf}.$$

Properties of the approximate Riemann solver

Well-balanced property

If $\mathbf{V}_{Lf}$ and $\mathbf{V}_{Rf}$ verify the steady "lake at rest" solution, we ask for

$$\mathbf{V}^{\star}_{Lf} = \mathbf{V}_{Lf} \quad \text{and} \quad \mathbf{V}^{\star}_{Rf} = \mathbf{V}_{Rf}.$$

We only need to impose **consistent definition** of the source term:

$$g\overline{h\Delta B}_{LR} = g\frac{h_R + h_L}{2}(B_R - B_L).$$

Properties of the approximate Riemann solver

Well-balanced property

If $\mathbf{V}_{Lf}$ and $\mathbf{V}_{Rf}$ verify the steady "lake at rest" solution, we ask for

$$\mathbf{V}^{\star}_{Lf} = \mathbf{V}_{Lf} \quad \text{and} \quad \mathbf{V}^{\star}_{Rf} = \mathbf{V}_{Rf}.$$

We only need to impose **consistent definition** of the source term:

$$g\overline{h\Delta B}_{LR} = g\frac{h_R + h_L}{2}(B_R - B_L).$$

Positivity-preserving and **entropy-stability** properties

To impose them, we **restrict** the values of the wave speeds **from below**.

Properties of the approximate Riemann solver

Well-balanced property

If $\mathbf{V}_{Lf}$ and $\mathbf{V}_{Rf}$ verify the steady "lake at rest" solution, we ask for

$$\mathbf{V}^{\star}_{Lf} = \mathbf{V}_{Lf} \quad \text{and} \quad \mathbf{V}^{\star}_{Rf} = \mathbf{V}_{Rf}.$$

We only need to impose **consistent definition** of the source term:

$$g\overline{h\Delta B}_{LR} = g\frac{h_R + h_L}{2}(B_R - B_L).$$

Positivity-preserving and **entropy-stability** properties

To impose them, we **restrict** the values of the wave speeds **from below**. These conditions are implicit: an iterative procedure is required.

- Positivity: $\lambda_L \geq -\dfrac{u^{\star}_{\mathbf{n}} - u_{\mathbf{n},L}}{\tau_L}$ and $\lambda_R \geq \dfrac{u^{\star}_{\mathbf{n}} - u_{\mathbf{n},R}}{\tau_R}$
- Entropy: $\lambda_L \geq \sqrt{g h^{\star}_L h_L}$ and $\lambda_R \geq \sqrt{g h^{\star}_R h_R}$

Eulerian approximate Riemann solver[5]

[5] [Chan et al. (2021)]

Eulerian approximate Riemann solver[5]

Jump relations for mass equation

$$u_{\mathbf{n},L} - \lambda_L \tau_L = u_{\mathbf{n}}^\star - \lambda_L \tau_L^\star, \qquad u_{\mathbf{n}}^\star, \qquad u_{\mathbf{n}}^\star + \lambda_R \tau_R^\star = u_{\mathbf{n},r} + \lambda_R \tau_R.$$

[5] [Chan et al. (2021)]

Eulerian approximate Riemann solver[5]

Eulerian wave speeds

Provided the positivity of specific volumes, $\tau_S^\star \geq 0$, the Eulerian wave speeds are ordered: $\Lambda_L \leq \Lambda_0 \leq \Lambda_R$:

$$\Lambda_L = u_{\mathbf{n},L} - \lambda_L \tau_L = u_{\mathbf{n}}^\star - \lambda_L \tau_L^\star, \quad \Lambda_0 = u_{\mathbf{n}}^\star, \quad \Lambda_R = u_{\mathbf{n}}^\star + \lambda_R \tau_R^\star = u_{\mathbf{n},r} + \lambda_R \tau_R.$$

[5] [Chan et al. (2021)]

Eulerian approximate Riemann solver[5]

Eulerian wave speeds

Provided the positivity of specific volumes, $\tau_S^\star \geq 0$, the Eulerian wave speeds are ordered: $\Lambda_L \leq \Lambda_0 \leq \Lambda_R$:

$$\Lambda_L = u_{\mathbf{n},L} - \lambda_L \tau_L = u_{\mathbf{n}}^\star - \lambda_L \tau_L^\star, \quad \Lambda_0 = u_{\mathbf{n}}^\star, \quad \Lambda_R = u_{\mathbf{n}}^\star + \lambda_R \tau_R^\star = u_{\mathbf{n},r} + \lambda_R \tau_R.$$

Eulerian approximate Riemann solver

$$\mathbf{W}_{\mathcal{E}} = \begin{cases} \mathbf{U}_L & \text{if} \quad \frac{x_{\mathbf{n}}}{t} \leq \Lambda_L, \\ \mathbf{U}_L^\star = \mathbf{U}(\mathbf{V}_L^\star) & \text{if} \quad \Lambda_L < \frac{x_{\mathbf{n}}}{t} \leq \Lambda_0, \\ \mathbf{U}_R^\star = \mathbf{U}(\mathbf{V}_R^\star) & \text{if} \quad \Lambda_0 < \frac{x_{\mathbf{n}}}{t} \leq \Lambda_R, \\ \mathbf{U}_R & \text{if} \quad \Lambda_R < \frac{x_{\mathbf{n}}}{t}. \end{cases}$$

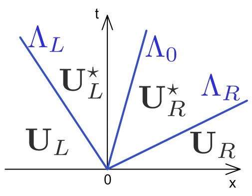

with Lagrange-to-Euler mapping $\mathbf{V} \mapsto \mathbf{U}(\mathbf{V})$.

[5] [Chan et al. (2021)]

Eulerian approximate Riemann solver[5]

Eulerian wave speeds

Provided the positivity of specific volumes, $\tau_S^\star \geq 0$, the Eulerian wave speeds are ordered: $\Lambda_L \leq \Lambda_0 \leq \Lambda_R$:

$$\Lambda_L = u_{\mathbf{n},L} - \lambda_L \tau_L = u_{\mathbf{n}}^\star - \lambda_L \tau_L^\star, \quad \Lambda_0 = u_{\mathbf{n}}^\star, \quad \Lambda_R = u_{\mathbf{n}}^\star + \lambda_R \tau_R^\star = u_{\mathbf{n},r} + \lambda_R \tau_R.$$

Eulerian approximate Riemann solver

$$\mathbf{W}_{\mathcal{E}} = \begin{cases} \mathbf{U}_L & \text{if} \quad \frac{x_{\mathbf{n}}}{t} \leq \Lambda_L, \\ \mathbf{U}_L^\star = \mathbf{U}(\mathbf{V}_L^\star) & \text{if} \quad \Lambda_L < \frac{x_{\mathbf{n}}}{t} \leq \Lambda_0, \\ \mathbf{U}_R^\star = \mathbf{U}(\mathbf{V}_R^\star) & \text{if} \quad \Lambda_0 < \frac{x_{\mathbf{n}}}{t} \leq \Lambda_R, \\ \mathbf{U}_R & \text{if} \quad \Lambda_R < \frac{x_{\mathbf{n}}}{t}. \end{cases}$$

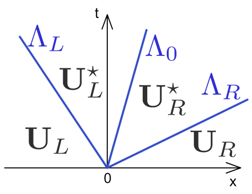

with Lagrange-to-Euler mapping $\mathbf{V} \mapsto \mathbf{U}(\mathbf{V})$.

$$\mathbf{U}_{\mathbf{n},Sf}^\star = \rho_{Sf}^\star \mathbf{V}_{\mathbf{n},Sf}^\star \quad \text{and} \quad \mathbf{F}_{\mathbf{n},Sf}^\star = u_{\mathbf{n}}^\star \mathbf{U}_{\mathbf{n},Sf}^\star + \mathbf{G}_{\mathbf{n},Sf}^\star \quad \text{with} \quad S = L, R.$$

[5] [Chan et al. (2021)]

Associated Godunov-type multi-point flux

$$\mathbf{U}_c^{n+1} = \mathbf{U}_c^n - \frac{\Delta t}{|\omega_c|} \sum_{p \in \mathcal{P}(c)} \sum_{f \in \mathcal{SF}(pc)} l_{pcf} \widetilde{\mathbf{F}}_{pcf}$$

$$\widetilde{\mathbf{F}}_{\mathbf{n}_{pcf}} = \mathbb{F}(\mathbf{U}_{Lf})\mathbf{n}_{pcf} - \int_{-\infty}^{0} \left[\mathbf{W}_{pcf,\mathcal{E}}(\mathbf{U}_{Lf}, \mathbf{U}_{Rf}, B_{Lf}, B_{Rf}, \mathbf{n}_{pcf}, \xi, \mathbf{u}_p) - \mathbf{U}_{Lf} \right] \, \mathrm{d}\xi$$

Associated Godunov-type multi-point flux

$$\mathbf{U}_c^{n+1} = \mathbf{U}_c^n - \frac{\Delta t}{|\omega_c|} \sum_{p \in \mathcal{P}(c)} \sum_{f \in \mathcal{SF}(pc)} l_{pcf} \widetilde{\mathbf{F}}_{pcf}$$

$$\widetilde{\mathbf{F}}_{\mathbf{n}_{pcf}} = \mathbb{F}(\mathbf{U}_{Lf})\mathbf{n}_{pcf} - \int_{-\infty}^{0} \left[\mathbf{W}_{pcf,\mathcal{E}}(\mathbf{U}_{Lf}, \mathbf{U}_{Rf}, B_{Lf}, B_{Rf}, \mathbf{n}_{pcf}, \xi, \mathbf{u}_p) - \mathbf{U}_{Lf} \right] \, \mathrm{d}\xi$$

$$\widetilde{\mathbf{F}}_{\mathbf{n}_{pcf}} = \frac{1}{2}\left[\mathbf{F}_{\mathbf{n}_{pcf}}(\mathbf{U}_c) + \mathbf{F}_{\mathbf{n}_{pcf}}(\mathbf{U}_d)\right] - \frac{1}{2}\left[\sum_{k=1}^{m} |\Lambda_k| (\mathbf{U}_{k+1} - \mathbf{U}_k)\right]_{c,d}$$
$$- \frac{\lambda_{L,pcf} + \lambda_{R,pcf}}{2} \left[\mathbf{u}_p \cdot \mathbf{n}_{pcf} - u_{\mathbf{n}_{pcf}}^{Godv,ws}\right] \mathbf{e}_2$$

Associated Godunov-type multi-point flux

$$\mathbf{U}_c^{n+1} = \mathbf{U}_c^n - \frac{\Delta t}{|\omega_c|} \sum_{p \in \mathcal{P}(c)} \sum_{f \in \mathcal{SF}(pc)} l_{pcf} \widetilde{\mathbf{F}}_{pcf}$$

$$\widetilde{\mathbf{F}}_{\mathbf{n}_{pcf}} = \mathbb{F}(\mathbf{U}_{Lf})\mathbf{n}_{pcf} - \int_{-\infty}^{0} \left[\mathbf{W}_{pcf,\mathcal{E}}(\mathbf{U}_{Lf}, \mathbf{U}_{Rf}, B_{Lf}, B_{Rf}, \mathbf{n}_{pcf}, \xi, \mathbf{u}_p) - \mathbf{U}_{Lf}\right] \, \mathrm{d}\xi$$

$$\begin{aligned}\widetilde{\mathbf{F}}_{\mathbf{n}_{pcf}} &= \frac{1}{2}\left[\mathbf{F}_{\mathbf{n}_{pcf}}(\mathbf{U}_c) + \mathbf{F}_{\mathbf{n}_{pcf}}(\mathbf{U}_d)\right] - \frac{1}{2}\left[\sum_{k=1}^{m} |\Lambda_k| (\mathbf{U}_{k+1} - \mathbf{U}_k)\right]_{c,d} \\ &\quad - \frac{\lambda_{L,pcf} + \lambda_{R,pcf}}{2}\left[\mathbf{u}_p \cdot \mathbf{n}_{pcf} - u_{\mathbf{n}_{pcf}}^{Godv,ws}\right] \mathbf{e}_2 \\ &= \overline{\mathbf{F}}_{\mathbf{n}_{pcf}}^{2P} - \frac{\lambda_{L,pcf} + \lambda_{R,pcf}}{2}\left[\mathbf{u}_p \cdot \mathbf{n}_{pcf} - u_{\mathbf{n}_{pcf}}^{Godv,ws}\right] \mathbf{e}_2\end{aligned}$$

Associated Godunov-type multi-point flux

$$\mathbf{U}_c^{n+1} = \mathbf{U}_c^n - \frac{\Delta t}{|\omega_c|} \sum_{p \in \mathcal{P}(c)} \sum_{f \in \mathcal{SF}(pc)} l_{pcf} \widetilde{\mathbf{F}}_{pcf}$$

$$\widetilde{\mathbf{F}}_{\mathbf{n}_{pcf}} = \mathbb{F}(\mathbf{U}_{Lf})\mathbf{n}_{pcf} - \int_{-\infty}^{0} \left[\mathbf{W}_{pcf,\varepsilon}(\mathbf{U}_{Lf}, \mathbf{U}_{Rf}, B_{Lf}, B_{Rf}, \mathbf{n}_{pcf}, \xi, \mathbf{u}_p) - \mathbf{U}_{Lf}\right] \, \mathrm{d}\xi$$

$$\begin{aligned} \widetilde{\mathbf{F}}_{\mathbf{n}_{pcf}} &= \frac{1}{2}\left[\mathbf{F}_{\mathbf{n}_{pcf}}(\mathbf{U}_c) + \mathbf{F}_{\mathbf{n}_{pcf}}(\mathbf{U}_d)\right] - \frac{1}{2}\left[\sum_{k=1}^{m} |\Lambda_k| (\mathbf{U}_{k+1} - \mathbf{U}_k)\right]_{c,d} \\ &\quad - \frac{\lambda_{L,pcf} + \lambda_{R,pcf}}{2}\left[\mathbf{u}_p \cdot \mathbf{n}_{pcf} - u_{\mathbf{n}_{pcf}}^{Godv,ws}\right] \mathbf{e}_2 \\ &= \overline{\mathbf{F}}_{\mathbf{n}_{pcf}}^{2P} - \frac{\lambda_{L,pcf} + \lambda_{R,pcf}}{2}\left[\mathbf{u}_p \cdot \mathbf{n}_{pcf} - u_{\mathbf{n}_{pcf}}^{Godv,ws}\right] \mathbf{e}_2 \end{aligned}$$

Associated Godunov-type multi-point flux

$$\mathbf{U}_c^{n+1} = \mathbf{U}_c^n - \frac{\Delta t}{|\omega_c|} \sum_{p \in \mathcal{P}(c)} \sum_{f \in \mathcal{SF}(pc)} l_{pcf} \widetilde{\mathbf{F}}_{pcf}$$

$$\widetilde{\mathbf{F}}_{\mathbf{n}_{pcf}} = \mathbb{F}(\mathbf{U}_{Lf})\mathbf{n}_{pcf} - \int_{-\infty}^{0} \left[\mathbf{W}_{pcf,\mathcal{E}}(\mathbf{U}_{Lf}, \mathbf{U}_{Rf}, B_{Lf}, B_{Rf}, \mathbf{n}_{pcf}, \xi, \mathbf{u}_p) - \mathbf{U}_{Lf}\right] \,\mathrm{d}\xi$$

$$\begin{aligned}\widetilde{\mathbf{F}}_{\mathbf{n}_{pcf}} &= \frac{1}{2}\left[\mathbf{F}_{\mathbf{n}_{pcf}}(\mathbf{U}_c) + \mathbf{F}_{\mathbf{n}_{pcf}}(\mathbf{U}_d)\right] - \frac{1}{2}\left[\sum_{k=1}^{m} |\Lambda_k|(\mathbf{U}_{k+1} - \mathbf{U}_k)\right]_{c,d} \\ &\quad - \frac{\lambda_{L,pcf} + \lambda_{R,pcf}}{2}\left[\mathbf{u}_p \cdot \mathbf{n}_{pcf} - u_{\mathbf{n}_{pcf}}^{Godv,ws}\right] \mathbf{e}_2 \\ &= \overline{\mathbf{F}}_{\mathbf{n}_{pcf}}^{2P} - \frac{\lambda_{L,pcf} + \lambda_{R,pcf}}{2}\left[\mathbf{u}_p \cdot \mathbf{n}_{pcf} - u_{\mathbf{n}_{pcf}}^{Godv}\right] \mathbf{e}_2 + \frac{1}{2} g\overline{h\Delta B}_{LR,pf}\mathbf{e}_2\end{aligned}$$

Associated Godunov-type multi-point flux

$$\mathbf{U}_c^{n+1} = \mathbf{U}_c^n - \frac{\Delta t}{|\omega_c|} \sum_{p \in \mathcal{P}(c)} \sum_{f \in \mathcal{SF}(pc)} l_{pcf} \left[l_{pcf} \overline{\mathbf{F}}_{pcf} - w_{pcf} \overline{\mathbf{S}}_{pcf} \right]$$

$$\widetilde{\mathbf{F}}_{\mathbf{n}_{pcf}} = \mathbb{F}(\mathbf{U}_{Lf})\mathbf{n}_{pcf} - \int_{-\infty}^{0} \left[\mathbf{W}_{pcf,\mathcal{E}}(\mathbf{U}_{Lf}, \mathbf{U}_{Rf}, B_{Lf}, B_{Rf}, \mathbf{n}_{pcf}, \xi, \mathbf{u}_p) - \mathbf{U}_{Lf} \right] \mathrm{d}\xi$$

$$\begin{aligned}
\widetilde{\mathbf{F}}_{\mathbf{n}_{pcf}} &= \frac{1}{2} \left[\mathbf{F}_{\mathbf{n}_{pcf}}(\mathbf{U}_c) + \mathbf{F}_{\mathbf{n}_{pcf}}(\mathbf{U}_d) \right] - \frac{1}{2} \left[\sum_{k=1}^{m} |\Lambda_k| (\mathbf{U}_{k+1} - \mathbf{U}_k) \right]_{c,d} \\
&\quad - \frac{\lambda_{L,pcf} + \lambda_{R,pcf}}{2} \left[\mathbf{u}_p \cdot \mathbf{n}_{pcf} - u_{\mathbf{n}_{pcf}}^{Godv,ws} \right] \mathbf{e}_2 \\
&= \overline{\mathbf{F}}^{2P}_{\mathbf{n}_{pcf}} - \frac{\lambda_{L,pcf} + \lambda_{R,pcf}}{2} \left[\mathbf{u}_p \cdot \mathbf{n}_{pcf} - u_{\mathbf{n}_{pcf}}^{Godv} \right] \mathbf{e}_2 + \frac{1}{2} g \overline{h \Delta B}_{LR,pf} \mathbf{e}_2 \\
&= \overline{\mathbf{F}}_{\mathbf{n}_{pcf}} + \frac{1}{2} g \overline{h \Delta B}_{LR,pf} \mathbf{e}_2
\end{aligned}$$

Numerical simulations

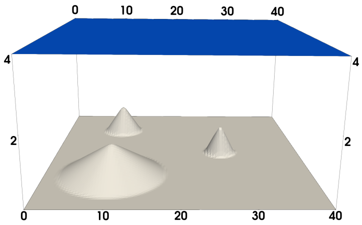

(a) 3D view of $h + B$ and B.

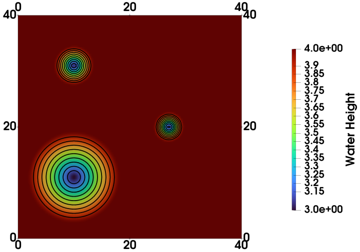

(b) Iso-lines of h.

- Preservation of steady state ✓
- Perturbation of steady state ✓

Radial dam break [6]

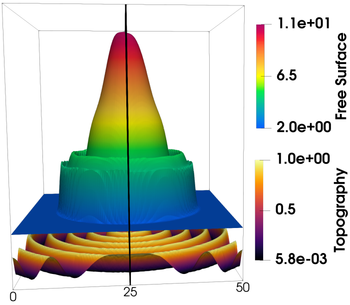

(c) 3D view of $h + B$ and B.

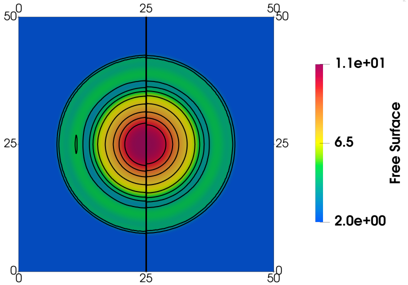

(d) 10 iso-lines of $2\text{m} < h + B < 11\text{m}$.

Initial conditions: $\mathbf{u} = \mathbf{0}$,

$$h(\mathbf{x}, t = 0) = \begin{cases} 11 - B(\mathbf{x}) & \text{if} \quad r \leq r_0, \\ 2 - B(\mathbf{x}) & \text{otherwise,} \end{cases} \quad \text{with} \quad B(\mathbf{x}) = \frac{1}{2}\left(1 + \cos\left(\frac{2\pi r}{2}\right)\right).$$

[6] [Alcrudo et al. (1993)]

Flow past a cylinder: Carbuncle[7]

The Carbuncle phenomenon is a **numerical artifact** that may appear in presence of **strong shocks** in **supersonic** and hypersonic regimes for the Euler equations.

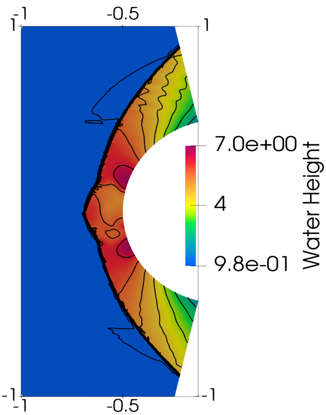

(e) Unstable scheme

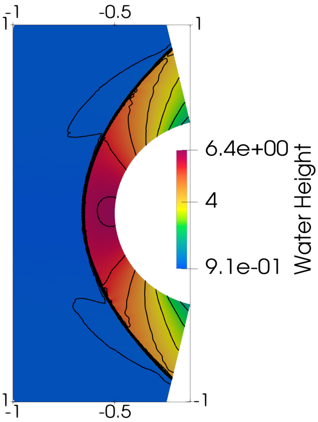

(f) Multi-point scheme: correct solution

[7] [Kemm (2014)]

Odd-even decoupling[8]

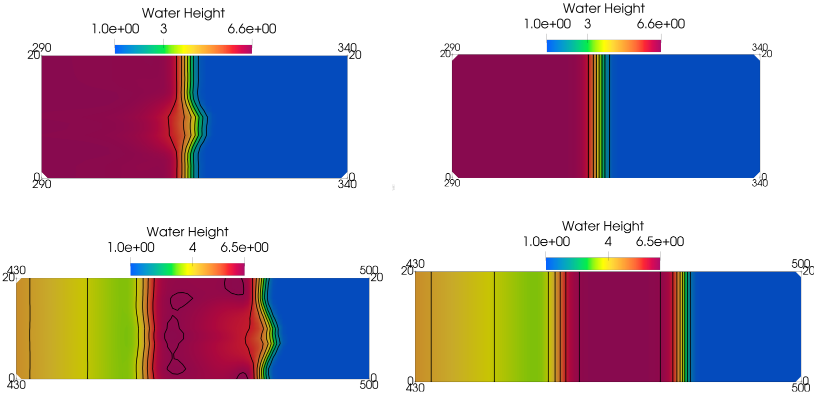

(g) Unstable scheme (h) Multi-point scheme: correct solution

We introduce a small **perturbation** of order 10^{-3} in the horizontal central grid line. This instability is considered of the same nature of the one in the blunt body problem.

[8] [Quirk (1994)]

A troublesome phenomenon: the Carbunçle [9]

There is not yet a unique opinion that has been adopted by everyone.

[9] [Quirk (1994), Pandolfi and D'Ambrosio (2001), Liou (2000), Dumbser et al. (2004), Kim t al. (2003), Robinet et al. (2000), Gressier and Moschetta (2000), Shen et al. (2016)]

A troublesome phenomenon: the Carbuncle [9]

There is not yet a unique opinion that has been adopted by everyone.

- Are complete Riemann solvers better than incomplete ones?

[9] [Quirk (1994), Pandolfi and D'Ambrosio (2001), Liou (2000), Dumbser et al. (2004), Kim t al. (2003), Robinet et al. (2000), Gressier and Moschetta (2000), Shen et al. (2016)]

A troublesome phenomenon: the Carbuncle [9]

There is not yet a unique opinion that has been adopted by everyone.

- Are complete Riemann solvers better than incomplete ones?
- Is the Carbuncle due to **insufficient dissipation**?

[9] [Quirk (1994), Pandolfi and D'Ambrosio (2001), Liou (2000), Dumbser et al. (2004), Kim t al. (2003), Robinet et al. (2000), Gressier and Moschetta (2000), Shen et al. (2016)]

A troublesome phenomenon: the Carbuncle [9]

There is not yet a unique opinion that has been adopted by everyone.

- Are complete Riemann solvers better than incomplete ones?
- Is the Carbuncle due to **insufficient dissipation**?
- It is generally believed that a numerical scheme that exactly solves **contact discontinuities** is prone to the Carbuncle.

[9] [Quirk (1994), Pandolfi and D'Ambrosio (2001), Liou (2000), Dumbser et al. (2004), Kim t al. (2003), Robinet et al. (2000), Gressier and Moschetta (2000), Shen et al. (2016)]

A troublesome phenomenon: the Carbuncle [9]

There is not yet a unique opinion that has been adopted by everyone.

- Are complete Riemann solvers better than incomplete ones?
- Is the Carbuncle due to **insufficient dissipation**?
- It is generally believed that a numerical scheme that exactly solves **contact discontinuities** is prone to the Carbuncle.
- The multi-point scheme preserves contact discontinuities but it is also Carbuncle-free.

[9] [Quirk (1994), Pandolfi and D'Ambrosio (2001), Liou (2000), Dumbser et al. (2004), Kim t al. (2003), Robinet et al. (2000), Gressier and Moschetta (2000), Shen et al. (2016)]

A troublesome phenomenon: the Carbuncle [9]

There is not yet a unique opinion that has been adopted by everyone.

- Are complete Riemann solvers better than incomplete ones?
- Is the Carbuncle due to **insufficient dissipation**?
- It is generally believed that a numerical scheme that exactly solves **contact discontinuities** is prone to the Carbuncle.
- The multi-point scheme preserves contact discontinuities but it is also Carbuncle-free.
- Similar conclusion about **shear lines**?

[9] [Quirk (1994), Pandolfi and D'Ambrosio (2001), Liou (2000), Dumbser et al. (2004), Kim t al. (2003), Robinet et al. (2000), Gressier and Moschetta (2000), Shen et al. (2016)]

A troublesome phenomenon: the Carbuncle [9]

There is not yet a unique opinion that has been adopted by everyone.

- Are complete Riemann solvers better than incomplete ones?
- Is the Carbuncle due to **insufficient dissipation**?
- It is generally believed that a numerical scheme that exactly solves **contact discontinuities** is prone to the Carbuncle.
- The multi-point scheme preserves contact discontinuities but it is also Carbuncle-free.
- Similar conclusion about **shear lines**?

  The multi-point scheme does **not** preserve shear lines due to the additional diffusion term in the flux definition:

$$\overline{\mathbf{F}}^{MP}_{\mathbf{n}_{pcf}} = \overline{\mathbf{F}}^{2P}_{\mathbf{n}_{pcf}} - \frac{\lambda_{L,pcf} + \lambda_{R,pcf}}{2} \left(\mathbf{u}_p \cdot \mathbf{n}_{pcf} - u^{Godv}_{\mathbf{n}_{pcf}} \right) \mathbf{e}_2$$

[9] [Quirk (1994), Pandolfi and D'Ambrosio (2001), Liou (2000), Dumbser et al. (2004), Kim t al. (2003), Robinet et al. (2000), Gressier and Moschetta (2000), Shen et al. (2016)]

Multi-dimensional origin [10]

Quirk (1994): the Carbuncle arises due to a lack of dissipation via the contact discontinuity in the direction parallel to the shock.

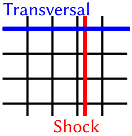

[10] [Sanders et al. (1998), Robinet et al. (2000), Dumbser et al. (2004), Moschetta et al. (2001), Morton and Roe (2001), Wada and Liou (1997), Chauvat et al. (2005), Jin and Liu (1996), Arora and Roe (1997), Bultelle et al. (1998), Zaide and Roe (2011), Zaide (2012)]

Multi-dimensional origin [10]

Quirk (1994): the Carbuncle arises due to a lack of dissipation via the contact discontinuity in the direction parallel to the shock.

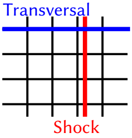

- Sanders et al. (1998): to extend a 1D numerical scheme to multi-dimension by simply applying a **dimensional flux-splitting** may lead to the Carbuncle.
- **Vorticity wave** to stabilize the numerical solutions: Moschetta et al., Dumbser et al., Morton and Roe...

[10] [Sanders et al. (1998), Robinet et al. (2000), Dumbser et al. (2004), Moschetta et al. (2001), Morton and Roe (2001), Wada and Liou (1997), Chauvat et al. (2005), Jin and Liu (1996), Arora and Roe (1997), Bultelle et al. (1998), Zaide and Roe (2011), Zaide (2012)]

Multi-dimensional origin [10]

Quirk (1994): the Carbuncle arises due to a lack of dissipation via the contact discontinuity in the direction parallel to the shock.

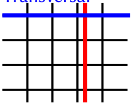

- Sanders et al. (1998): to extend a 1D numerical scheme to multi-dimension by simply applying a **dimensional flux-splitting** may lead to the Carbuncle.
- **Vorticity wave** to stabilize the numerical solutions: Moschetta et al., Dumbser et al., Morton and Roe...
- The **numerical structure of shocks**: physical shocks are numerically represented by various points → intermediate ones are purely numerical
  Wada and Liou (1997) supposed that these **intermediate points may exchange information** with the neighbors. See also Dumbser et al., Chauvat et al.

[10] [Sanders et al. (1998), Robinet et al. (2000), Dumbser et al. (2004), Moschetta et al. (2001), Morton and Roe (2001), Wada and Liou (1997), Chauvat et al. (2005), Jin and Liu (1996), Arora and Roe (1997), Bultelle et al. (1998), Zaide and Roe (2011), Zaide (2012)]

Multi-dimensional origin [10]

Quirk (1994): the Carbuncle arises due to a lack of dissipation via the contact discontinuity in the direction parallel to the shock.

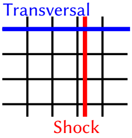

- Sanders et al. (1998): to extend a 1D numerical scheme to multi-dimension by simply applying a **dimensional flux-splitting** may lead to the Carbuncle.
- **Vorticity wave** to stabilize the numerical solutions: Moschetta et al., Dumbser et al., Morton and Roe...
- The **numerical structure of shocks**: physical shocks are numerically represented by various points $\rightarrow$ intermediate ones are purely numerical
  Wada and Liou (1997) supposed that these **intermediate points may exchange information** with the neighbors. See also Dumbser et al., Chauvat et al.
- **Has Carbuncle 1D roots**? Jin and Liu, Arora and Roe, Bultelle et al., Zaide, etc.
  Zaide and Roe (2011) studied the **relations of the non-linearity of the Rankine-Hugoniot conditions** with the shock instability in 1D.

[10] [Sanders et al. (1998), Robinet et al. (2000), Dumbser et al. (2004), Moschetta et al. (2001), Morton and Roe (2001), Wada and Liou (1997), Chauvat et al. (2005), Jin and Liu (1996), Arora and Roe (1997), Bultelle et al. (1998), Zaide and Roe (2011), Zaide (2012)]

What is the root of the Carbuncle phenomenon?[11]

Physical origin

- Researchers have carried out experiments in which they tried to induce the Carbuncle phenomenon in the numerical solution.

[11] [Dumbser et al. (2004), Elling (2009), Morton and Roe (2001), Gressier and Moschetta (2000), Robinet et al. (2000)]

What is the root of the Carbuncle phenomenon?[11]

Physical origin

- Researchers have carried out experiments in which they tried to induce the Carbuncle phenomenon in the numerical solution.
- This suggests that the **Carbuncle is not a purely numerical artifact**: it can be the **correct physical solution**. The unphysical Carbuncle may be a different **entropy-satisfying solution** for the same data.

[11] [Dumbser et al. (2004), Elling (2009), Morton and Roe (2001), Gressier and Moschetta (2000), Robinet et al. (2000)]

What is the root of the Carbuncle phenomenon?[11]

Physical origin

- Researchers have carried out experiments in which they tried to induce the Carbuncle phenomenon in the numerical solution.
- This suggests that the **Carbuncle is not a purely numerical artifact**: it can be the **correct physical solution**. The unphysical Carbuncle may be a different **entropy-satisfying solution** for the same data.
- Elling (2009) uses "**filaments**" to trigger the Carbuncle at the shock level.

[11] [Dumbser et al. (2004), Elling (2009), Morton and Roe (2001), Gressier and Moschetta (2000), Robinet et al. (2000)]

Elling test [12]

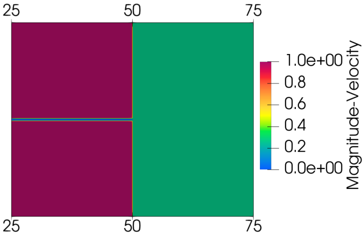

(i) Initial condition

[12] [Fleischmann et al. (2022)]

Elling test [12]

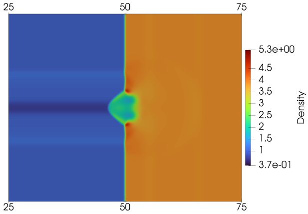

(a) HLL scheme (1600 × 640 cells)

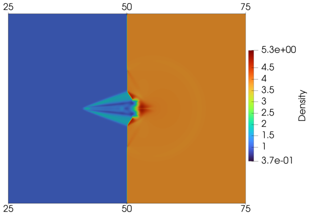

(b) 2point scheme (1600 × 640 cells)

[12][Fleischmann et al. (2022)]

Elling test [12]

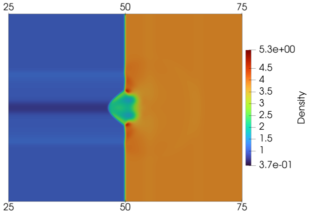

(a) HLL scheme (1600 × 640 cells)

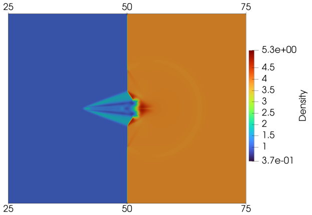

(b) 2point scheme (1600 × 640 cells)

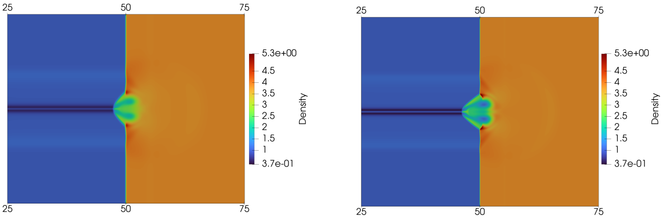

Figure: Multi-point scheme. 800 × 320 (right) and 1600 × 640 (left) cells.

[12] [Fleischmann et al. (2022)]

What is the root of the Carbuncle phenomenon?[13]

Physical origin

- Researchers have carried out experiments in which they tried to induce the Carbuncle phenomenon in the numerical solution.
- This suggests that the **Carbuncle is not a purely numerical artifact**: it can be the **correct physical solution**. The unphysical Carbuncle may be a different **entropy-satisfying solution** for the same data.
- Elling (2009) uses "filaments" which triggers the Carbuncle at the shock level.

[13] [Dumbser et al. (2004), Elling (2009), Morton and Roe (2001), Gressier and Moschetta (2000), Robinet et al. (2000)]

What is the root of the Carbuncle phenomenon?[13]

Physical origin

- Researchers have carried out experiments in which they tried to induce the Carbuncle phenomenon in the numerical solution.
- This suggests that the **Carbuncle is not a purely numerical artifact**: it can be the **correct physical solution**. The unphysical Carbuncle may be a different **entropy-satisfying solution** for the same data.
- Elling (2009) uses "filaments" which triggers the Carbuncle at the shock level.
- A numerical scheme should be able to reproduce the **physical** Carbuncle but not the instability.

[13] [Dumbser et al. (2004), Elling (2009), Morton and Roe (2001), Gressier and Moschetta (2000), Robinet et al. (2000)]

What is the root of the Carbuncle phenomenon?[13]

Physical origin

- Researchers have carried out experiments in which they tried to induce the Carbuncle phenomenon in the numerical solution.
- This suggests that the **Carbuncle is not a purely numerical artifact**: it can be the **correct physical solution**. The unphysical Carbuncle may be a different **entropy-satisfying solution** for the same data.
- Elling (2009) uses "filaments" which triggers the Carbuncle at the shock level.
- A numerical scheme should be able to reproduce the **physical** Carbuncle but not the instability.
- Elling goes as far as to say that **Carbuncles are incurable**: trying to eliminate them implies assuming that the upstream flow is smooth, free of filaments and other disturbances.

[13] [Dumbser et al. (2004), Elling (2009), Morton and Roe (2001), Gressier and Moschetta (2000), Robinet et al. (2000)]

Many hypotheses/aspects...

- Pressure fluctuations
- Liou's (2000) conjecture
- Mach number in the transversal direction to the shock
- Entropy wave
- Perturbation downstream or upstream the shock
- Refinement of the grid
- High-order of accuracy

Many hypotheses/aspects...

- Pressure fluctuations
- Liou's (2000) conjecture
- Mach number in the transversal direction to the shock
- Entropy wave
- Perturbation downstream or upstream the shock
- Refinement of the grid
- High-order of accuracy

Is there a way to establish if a given scheme is prone to the Carbuncle?

Matrix stability analysis[14]

We consider a 2D planar steady shock and we analyse the **evolution of perturbation errors** by using the matrix method. Specifically, we compute the eigenvalues of the stability matrix and, depending on their value, classify the numerical scheme accordingly as Carbuncle-prone or not.

[14] [Dumbser et al. (2004)]

Matrix stability analysis[14]

We consider a 2D planar steady shock and we analyse the **evolution of perturbation errors** by using the matrix method. Specifically, we compute the eigenvalues of the stability matrix and, depending on their value, classify the numerical scheme accordingly as Carbuncle-prone or not.

- The **semi-discretization** of the Euler system reads

$$\frac{d\mathbf{U}_c}{dt} = -\frac{1}{|\omega_c|} \sum_{k \in \mathcal{FN}(c)} l_{ck} \overline{\mathbf{F}}_{ck} \tag{1}$$

[14] [Dumbser et al. (2004)]

Matrix stability analysis[14]

We consider a 2D planar steady shock and we analyse the **evolution of perturbation errors** by using the matrix method. Specifically, we compute the eigenvalues of the stability matrix and, depending on their value, classify the numerical scheme accordingly as Carbuncle-prone or not.

- The **semi-discretization** of the Euler system reads

$$\frac{d\mathbf{U}_c}{dt} = -\frac{1}{|\omega_c|} \sum_{k \in \mathcal{FN}(c)} l_{ck} \overline{\mathbf{F}}_{ck} \tag{1}$$

- Expand the field into its steady mean value ($\wedge$) and **error** (δ):

$$\mathbf{U}_c = \widehat{\mathbf{U}}_c + \delta \mathbf{U}_c$$

[14] [Dumbser et al. (2004)]

Matrix stability analysis[14]

We consider a 2D planar steady shock and we analyse the **evolution of perturbation errors** by using the matrix method. Specifically, we compute the eigenvalues of the stability matrix and, depending on their value, classify the numerical scheme accordingly as Carbuncle-prone or not.

- The **semi-discretization** of the Euler system reads

$$\frac{d\mathbf{U}_c}{dt} = -\frac{1}{|\omega_c|} \sum_{k \in \mathcal{FN}(c)} l_{ck} \overline{\mathbf{F}}_{ck} \tag{1}$$

- Expand the field into its steady mean value ($\wedge$) and **error** (δ):

$$\mathbf{U}_c = \widehat{\mathbf{U}}_c + \delta \mathbf{U}_c$$

- **Linearize $\overline{\mathbf{F}}_{ck}$** around the steady mean value

$$\overline{\mathbf{F}}_{ck}(\mathbf{U}_c, \mathbf{U}_k) = \overline{\mathbf{F}}_{ck}(\widehat{\mathbf{U}}_c, \widehat{\mathbf{U}}_k) + \frac{\partial \overline{\mathbf{F}}_{ck}}{\partial \mathbf{U}_c} \cdot \delta \mathbf{U}_c + \frac{\partial \overline{\mathbf{F}}_{ck}}{\partial \mathbf{U}_k} \cdot \delta \mathbf{U}_k$$

[14] [Dumbser et al. (2004)]

Matrix stability analysis

- **Linear error evolution model** reads

$$\frac{d(\delta \mathbf{U}_c)}{dt} = -\frac{1}{|\omega_c|} \sum_{k \in \mathcal{FN}(c)} l_{ck} \left[\frac{\partial \overline{\mathbf{F}}_{ck}}{\partial \mathbf{U}_c} \cdot \delta \mathbf{U}_c + \frac{\partial \overline{\mathbf{F}}_{ck}}{\partial \mathbf{U}_k} \cdot \delta \mathbf{U}_k \right] \tag{2}$$

- Error evolution

$$\frac{d}{dt} \begin{pmatrix} \delta \mathbf{U}_1 \\ \vdots \\ \delta \mathbf{U}_N \end{pmatrix} = \mathcal{S} \cdot \begin{pmatrix} \delta \mathbf{U}_1 \\ \vdots \\ \delta \mathbf{U}_N \end{pmatrix} \tag{3}$$

- $\mathcal{S}$ is the **stability matrix** of dimension $4N \times 4N$.

Matrix stability analysis

- **Linear error evolution model** reads

$$\frac{d(\delta \mathbf{U}_c)}{dt} = -\frac{1}{|\omega_c|} \sum_{k \in \mathcal{FN}(c)} l_{ck} \left[\frac{\partial \overline{\mathbf{F}}_{ck}}{\partial \mathbf{U}_c} \cdot \delta \mathbf{U}_c + \frac{\partial \overline{\mathbf{F}}_{ck}}{\partial \mathbf{U}_k} \cdot \delta \mathbf{U}_k \right] \tag{2}$$

- Error evolution

$$\frac{d}{dt} \begin{pmatrix} \delta \mathbf{U}_1 \\ \vdots \\ \delta \mathbf{U}_N \end{pmatrix} = \mathcal{S} \cdot \begin{pmatrix} \delta \mathbf{U}_1 \\ \vdots \\ \delta \mathbf{U}_N \end{pmatrix} \tag{3}$$

- $\mathcal{S}$ is the **stability matrix** of dimension $4N \times 4N$.
- The solution of (3) is

$$\begin{pmatrix} \delta \mathbf{U}_1 \\ \vdots \\ \delta \mathbf{U}_N \end{pmatrix} (t) = \exp(\mathcal{S} t) \begin{pmatrix} \delta \mathbf{U}_1 \\ \vdots \\ \delta \mathbf{U}_N \end{pmatrix}_{t=0}$$

Matrix stability analysis

- **Linear error evolution model** reads

$$\frac{d(\delta \mathbf{U}_c)}{dt} = -\frac{1}{|\omega_c|} \sum_{k \in \mathcal{FN}(c)} l_{ck} \left[\frac{\partial \overline{\mathbf{F}}_{ck}}{\partial \mathbf{U}_c} \cdot \delta \mathbf{U}_c + \frac{\partial \overline{\mathbf{F}}_{ck}}{\partial \mathbf{U}_k} \cdot \delta \mathbf{U}_k \right] \tag{2}$$

- Error evolution

$$\frac{d}{dt} \begin{pmatrix} \delta \mathbf{U}_1 \\ \vdots \\ \delta \mathbf{U}_N \end{pmatrix} = \mathcal{S} \cdot \begin{pmatrix} \delta \mathbf{U}_1 \\ \vdots \\ \delta \mathbf{U}_N \end{pmatrix} \tag{3}$$

- $\mathcal{S}$ is the **stability matrix** of dimension $4N \times 4N$.
- The solution of (3) is

$$\begin{pmatrix} \delta \mathbf{U}_1 \\ \vdots \\ \delta \mathbf{U}_N \end{pmatrix} (t) = \exp(\mathcal{S} t) \begin{pmatrix} \delta \mathbf{U}_1 \\ \vdots \\ \delta \mathbf{U}_N \end{pmatrix}_{t=0}$$

- The **sign of the eigenvalues** indicates how the error perturbation evolves:

$$\max(\mathrm{Re}(\lambda(\mathcal{S}))) \leq 0$$

Matrix stability analysis

- **Linear error evolution model** reads

$$\frac{d(\delta \mathbf{U}_c)}{dt} = -\frac{1}{|\omega_c|} \sum_{k \in \mathcal{FN}(c)} l_{ck} \left[\frac{\partial \overline{\mathbf{F}}_{ck}}{\partial \mathbf{U}_c} \cdot \delta \mathbf{U}_c + \frac{\partial \overline{\mathbf{F}}_{ck}}{\partial \mathbf{U}_k} \cdot \delta \mathbf{U}_k \right] \tag{2}$$

- Error evolution

$$\frac{d}{dt} \begin{pmatrix} \delta \mathbf{U}_1 \\ \vdots \\ \delta \mathbf{U}_N \end{pmatrix} = \mathcal{S} \cdot \begin{pmatrix} \delta \mathbf{U}_1 \\ \vdots \\ \delta \mathbf{U}_N \end{pmatrix} \tag{3}$$

- $\mathcal{S}$ is the **stability matrix** of dimension $4N \times 4N$.
- The solution of (3) is

$$\begin{pmatrix} \delta \mathbf{U}_1 \\ \vdots \\ \delta \mathbf{U}_N \end{pmatrix} (t) = \exp(\mathcal{S} t) \begin{pmatrix} \delta \mathbf{U}_1 \\ \vdots \\ \delta \mathbf{U}_N \end{pmatrix}_{t=0}$$

- The **sign of the eigenvalues** indicates how the error perturbation evolves:

$$\max(\mathrm{Re}(\lambda(\mathcal{S}))) \leq 0$$

- We extended this analysis for **multi-point** numerical schemes.

Matrix stability analysis

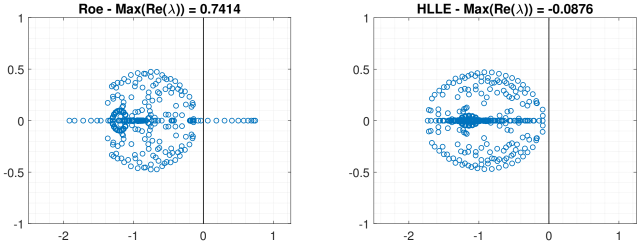

Figure: **Roe**'s scheme on the left. **HLLE** method on the right.

Matrix stability analysis

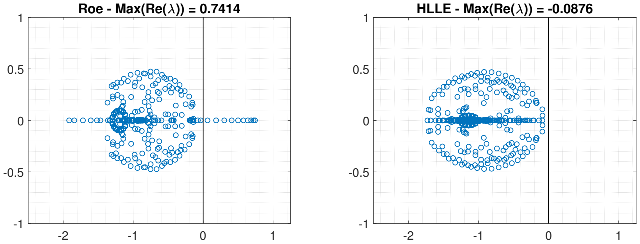

Figure: **Roe**'s scheme on the left. **HLLE** method on the right.

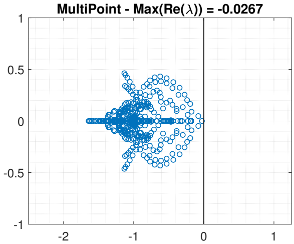

Figure: **Multi-point** scheme. 1D wave speeds on the left.

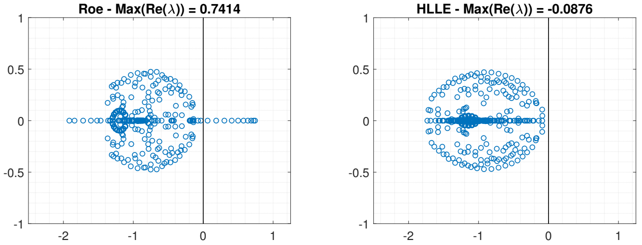

Figure: **Roe**'s scheme on the left. **HLLE** method on the right.

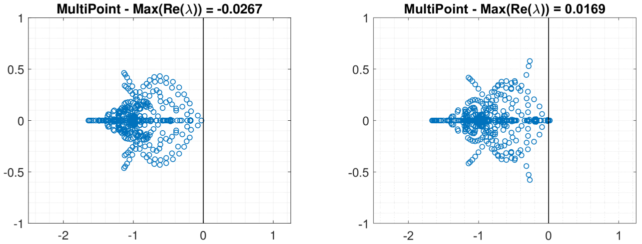

Figure: **Multi-point** scheme. 1D wave speeds on the left. Dukowicz wave speeds on the right.

Matrix stability analysis

Perturbations are inserted in the initial conditions in order to trigger instabilities.

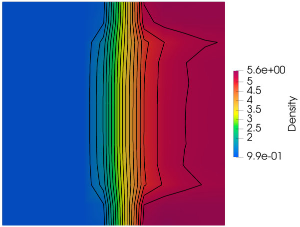

(a) Roe's scheme

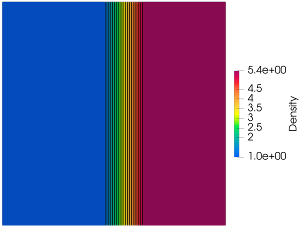

(b) Multi-point scheme, Dukowicz wave speeds

Conclusion?

Concluding remarks and perspectives

Conclusions

- The multi-point numerical scheme is well-balanced, positivity- and entropy-preserving;
- It is insensitive to the Carbuncle phenomenon;
- We suppose the diffusion related to the **shear lines** to be crucial;
- The analyses conducted so far give mixed results.

Concluding remarks and perspectives

Conclusions

- The multi-point numerical scheme is well-balanced, positivity- and entropy-preserving;
- It is insensitive to the Carbuncle phenomenon;
- We suppose the diffusion related to the **shear lines** to be crucial;
- The analyses conducted so far give mixed results.

Perspectives

- Further analysis of the method;
- Extension to more complex physics;
- Higher-order of accuracy;

Concluding remarks and perspectives

Conclusions

- The multi-point numerical scheme is well-balanced, positivity- and entropy-preserving;
- It is insensitive to the Carbuncle phenomenon;
- We suppose the diffusion related to the **shear lines** to be crucial;
- The analyses conducted so far give mixed results.

Perspectives

- Further analysis of the method;
- Extension to more complex physics;
- Higher-order of accuracy;
- **What about low-Mach flows?**

Current work for low-Mach flows[15]

- Low-Mach flows: $M = |u|/c \ll 1 \implies$ **flow velocity** $\ll$ **sound speed**
- Classical schemes fail to reproduce an accurate solution for **low-Mach flows**: **lack of consistency** with its limit behaviour as M tends to zero

[15] [Bourgeois et al. (2021), Barsukow et al. (2023), Chalons et al. (2017), Thomann et al. (2020)]

Current work for low-Mach flows[15]

- Low-Mach flows: $M = |u|/c \ll 1 \implies$ **flow velocity** $\ll$ **sound speed**
- Classical schemes fail to reproduce an accurate solution for **low-Mach flows**: **lack of consistency** with its limit behaviour as M tends to zero

Barsukow et al. (2023): multi-point scheme with **nodal pressure** to the linear acoustic equations

[15] [Bourgeois et al. (2021), Barsukow et al. (2023), Chalons et al. (2017), Thomann et al. (2020)]

Current work for low-Mach flows[15]

- Low-Mach flows: $M = |u|/c \ll 1 \implies$ **flow velocity** $\ll$ **sound speed**
- Classical schemes fail to reproduce an accurate solution for **low-Mach flows**: **lack of consistency** with its limit behaviour as M tends to zero

Barsukow et al. (2023): multi-point scheme with **nodal pressure** to the linear acoustic equations $\implies$ **Current work: extension to the Euler system**

[15] [Bourgeois et al. (2021), Barsukow et al. (2023), Chalons et al. (2017), Thomann et al. (2020)]

Current work for low-Mach flows[15]

- Low-Mach flows: $M = |u|/c \ll 1 \implies$ **flow velocity** $\ll$ **sound speed**
- Classical schemes fail to reproduce an accurate solution for **low-Mach flows**: **lack of consistency** with its limit behaviour as M tends to zero

Barsukow et al. (2023): multi-point scheme with **nodal pressure** to the linear acoustic equations $\implies$ **Current work: extension to the Euler system**

Problem: **not clear** how to move **from the Lagrangian** RS **to the Eulerian** RS due to the presence of two star velocities.

[15] [Bourgeois et al. (2021), Barsukow et al. (2023), Chalons et al. (2017), Thomann et al. (2020)]

Current work for low-Mach flows[15]

- Low-Mach flows: $M = |u|/c \ll 1 \implies$ **flow velocity** $\ll$ **sound speed**
- Classical schemes fail to reproduce an accurate solution for **low-Mach flows**: **lack of consistency** with its limit behaviour as M tends to zero

Barsukow et al. (2023): multi-point scheme with **nodal pressure** to the linear acoustic equations $\implies$ **Current work: extension to the Euler system**

Problem: **not clear** how to move **from the Lagrangian** RS **to the Eulerian** RS due to the presence of two star velocities.

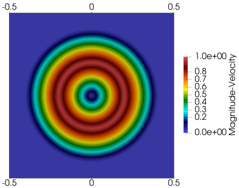

(o) Initial condition

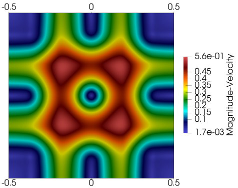

(p) Two-point scheme

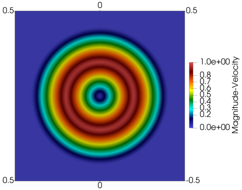

(q) New multi-point scheme

[15] [Bourgeois et al. (2021), Barsukow et al. (2023), Chalons et al. (2017), Thomann et al. (2020)]

Thank you for your attention!

References

F. Alcrudo and P. García-Navarro. *A high resolution Godunov-type scheme in finite volumes for the 2d shallow water equations.* International Journal for Numerical Methods in Fluids 16 (1993): 489-505.

M. Arora and P. L. Roe. *On postshock oscillations due to shock capturing schemes in unsteady flows.* Journal of Computational Physics, 130(1):25–40, 1997. 10.1006/jcph.1996.5534

E. Audusse, F. Bouchut, M.O. Bristeau, R. Klein and B. Perthame. *A fast and stable well-balanced scheme with hydrostatic reconstruction for shallow water flows.* SIAM Journal on Scientific Computing, 25: 2050-2065, 2004. 10.1137/S1064827503431090.

A node-conservative vorticity-preserving Finite Volume method for linear acoustics on unstructured grids. Submitted.

W. Barsukow, *Truly multi-dimensional all-speed schemes for the Euler equations on Cartesian grids.* Journal of Computational Physics, 435, 110216, ISSN 0021-9991, 2021. 10.1016/j.jcp.2021.110216.

R. Bourgeois, P. Tremblin, S. Kokh, T. Padioleau, *Recasting an operator splitting solver into a standard finite volume flux-based algorithm. The case of a Lagrange-projection-type method for gas dynamics.* Journal of Computational Physics, 496, 112594, ISSN 0021-9991, 2024. 10.1016/j.jcp.2023.112594.

References

- M. Bultelle, M. Grassin, and D. Serre. *Unstable Godunov discrete profiles for steady shock waves.* SIAM Journal on Numerical Analysis, 35(6):2272–2297, 1998. 10.1137/S0036142996312288
- C. Chalons, M. Girardin, and S. Kokh. *An all-regime lagrange-projection like scheme for the gas dynamics equations on unstructured meshes.* Communications in Computational Physics, 20, 06 2014. 10.4208/cicp.260614.061115a
- C. Chalons, M. Girardin, and S. Kokh. *An all-regime Lagrange-Projection like scheme for 2D homogeneous models for two-phase flows on unstructured meshes.* Journal of Computational Physics, 335:885–904, April 2017. 10.1016/j.jcp.2017.01.017
- A. Chan, G. Gallice, R. Loubère, P.-H. Maire, *Positivity preserving and entropy consistent approximate Riemann solvers dedicated to the high-order MOOD-based Finite Volume discretization of Lagrangian and Eulerian gas dynamics.* Computers & Fluids, 229, 105056, ISSN 0045-7930, 2021. 10.1016/j.compfluid.2021.105056.
- Y. Chauvat, J.-M. Moschetta, and J. Gressier. *Shock wave numerical structure and the carbuncle phenomenon.* International Journal for Numerical Methods in Fluids, 47(8-9):903–909, 2005. 10.1002/fld.916
- M. Dumbser, J.-M. Moschetta, and J. Gressier. *A matrix stability analysis of the carbuncle phenomenon.* Journal of Computational Physics, 197(2):647–670, 2004. 10.1016/j.jcp.2003.12.013

References

- M. Dumbser, J.-M. Moschetta, and J. Gressier. *A matrix stability analysis of the carbuncle phenomenon.* Journal of Computational Physics, 197(2):647–670, 2004. 10.1016/j.jcp.2003.12.013
- V. Elling. *The carbuncle phenomenon is incurable.* Acta Mathematica Scientia, 29(6):1647–1656, 2009. Mathematics Dedicated to professor James Glimm on the occasion of his 75th birthday. 10.1016/S0252-9602(10)60007-0
- N. Fleischmann, S. Adami, and N. A. Adams. *A shock-stable modification of the hllc riemann solver with reduced numerical dissipation.* Journal of Computational Physics, 423:109762, 2020. 10.1016/j.jcp.2020.109762
- N. Fleischmann, S. Adami, X. Hu, N Adams. *A low dissipation method to cure the grid-aligned shock instability.* Journal of Computational Physics. 401, 109004, 2020. 10.1016/j.jcp.2019.109004.
- G. Gallice, A. Chan, R. Loubère, P.-H. Maire. *Entropy Stable and Positivity Preserving Godunov-Type Schemes for Multidimensional Hyperbolic Systems on Unstructured Grid.* Journal of Computational Physics, 468, 111493, ISSN 0021-9991, 2022. 10.1016/j.jcp.2022.111493.
- G. Gallice. *Solveurs simples positifs et entropiques pour les systèmes hyperboliques avec terme source.* C. R. Math. Acad. Sci. Paris 334(8): 713-716, 2002. 10.1016/S1631-073X(02)02307-5.

References

- E. Godlewski, P.A. Raviart. *Numerical Approximation of Hyperbolic Systems of Conservation Laws.* Springer, 1996.
- J. Gressier and J.-M. Moschetta. *Robustness versus accuracy in shock-wave computations.* International Journal for Numerical Methods in Fluids, 33, 06 2000. 10.1002/1097-0363(20000615)33:33.0.CO;2-E
- H. Guillard and A. Murrone. *On the behavior of upwind schemes in the low mach number limit: Ii. Godunov type schemes.* Computers & Fluids, 33(4):655–675, 2004. 10.1016/j.compfluid.2003.07.001
- H. Guillard and C. Viozat. *On the behaviour of upwind schemes in the low mach number limit.* Computers & Fluids, 28(1):63–86, 1999. 10.1016/bs.hna.2016.09.002
- S. Jin and J.-G. Liu. *The effects of numerical viscosities: I. slowly moving shocks.* Journal of Computational Physics, 126(2):373–389, 1996. 10.1006/jcph.1996.0144
- F. Kemm. *A note on the carbuncle phenomenon in shallow water simulations.* ZAMM - Journal of Applied Mathematics and Mechanics / Zeitschrift für Angewandte Mathematik und Mechanik, 94, 2014.
- F. Kemm and G. Bader. *The Carbuncle Phenomenon in Shallow Water Simulations.* 2nd International Conference on Computational Science and Engineering, 2014.

References

F. Kemm. *Heuristical and numerical considerations for the carbuncle phenomenon.* Applied Mathematics and Computation, 320: 596-613, ISSN 0096-3003, 2018. 10.1016/j.amc.2017.09.014.

S. s. Kim, C. Kim, O.-H. Rho, and S. Kyu Hong. *Cures for the shock instability: Development of a shock-stable roe scheme.* Journal of Computational Physics, 185(2):342–374, 2003. 10.1016/S0021-9991(02)00037-2

P. Lax. *Hyperbolic Systems of Conservation Laws and Mathematical Theory Shock Waves.* Society for Industrial and Applied Mathematics, 1973. 10.1137/1.9781611970562.

P. LeFloch. *Entropy weak solutions to nonlinear hyperbolic systems under nonconservative form.* Communications in Partial Differential Equations. 13: 669-727, 1988. 10.1080/03605308808820557.

M.-S. Liou. *Mass flux schemes and connection to shock instability.* Journal of Computational Physics, 160(2):623–648, 2000. 10.1006/jcph.2000.6478

K. Morton and Philip Roe. *Vorticity-preserving Lax-Wendroff-type schemes for the system wave equation.* Siam Journal on Scientific Computing, 23, 06 2001. 10.1137/S106482759935914X

References

J.-M. Moschetta, J. Gressier, J.-C. Robinet, and G. Casalis. *The carbuncle phenomenon: A genuine euler instability ?* 01 2001. 10.1007/978-1-4615-0663-8_63

A. Navas-Montilla and J. Murillo. *2d well-balanced augmented ader schemes for the shallow water equations with bed elevation and extension to the rotating frame.* Journal of Computational Physics, 372:316–348, 2018. 10.1016/j.jcp.2018.06.039

Maurizio Pandolfi and Domenic D'Ambrosio. *Numerical instabilities in upwind methods: Analysis and cures for the "carbuncle" phenomenon.* Journal of Computational Physics, 166(2):271–301, 2001. 10.1006/jcph.2000.6652

K. Peery and S. Imlay. *Blunt-body flow simulations.* 1988. 10.2514/6.1988-2904

J. Quirk. *A Contribution to the Great Riemann Solver Debate.* International Journal for Numerical Methods in Fluids, 18: 555-574, 1994.

W. Ren, W. Xie, Y. Zhang, H. Yu, Z. Tian. *Numerical stability analysis of shock-capturing methods for strong shocks II: high-order finite-volume schemes.* https://arxiv.org/abs/2308.03428

J.-C. Robinet, J. Gressier, G. Casalis, and J.-M. Moschetta. *Shock wave instability and the carbuncle phenomenon: Same intrinsic origin?* Journal of Fluid Mechanics, 417:237 – 263, 08 2000. 10.1017/S0022112000001129

References

A. V. Rodionov. *Artificial viscosity in Godunov-type schemes to cure the carbuncle phenomenon.* J. Comput. Phys. 345: 308-329, 2017.

A. V. Rodionov. *Artificial viscosity to cure the shock instability in high-order godunov-type schemes.* Computers & Fluids, 190:77–97, 2019. 10.1016/j.compfluid.2019.06.011

R. Sanders, E. Morano, and M.-C. Druguet. *Multidimensional dissipation for upwind schemes: Stability and applications to gas dynamics.* Journal of Computational Physics, 145(2):511–537, 1998. 10.1006/jcph.1998.6047

S. Sangeeth. *Numerical Shock Instability In HLL-Based Approximate Riemann Solvers For The Euler System Of Equations: Analysis And Cures.* PhD thesis, 08 2019. 10.13140/RG.2.2.31946.52169

Z. Shen, W. Yan, G. Yuan, *A robust HLLC-type Riemann solver for strong shock.* Journal of Computational Physics, 309, 2016, 185-206, ISSN 0021-9991. 10.1016/j.jcp.2016.01.001.

R. Temam. *The Navier-Stokes Equations: Theory and Numerical Methods.* American Mathematical Society. 343, 2001.

A. Thomann, M. Zenk, G. Puppo, C. Klingenberg. *An All Speed Second Order IMEX Relaxation Scheme for the Euler Equations.* Communications in Computational Physics. 28. 591-620. 2020. 10.4208/cicp.OA-2019-0123.

References

- E. F. Toro. *Riemann Solvers and Numerical Methods for Fluid Dynamics*, Third Edition. Springer– Verlag, 2009. 10.1007/b79761_5.
- B. van Leer. *The Development of Numerical Fluid Mechanics and Aerodynamics since the 1960's: US and Canada*, 100, 159–185. 10.1007/978-3-540-70805-6_14
- C. B. Vreugdenhil. *Numerical Methods for Shallow Water Flow.* Dordrecht; Boston: Kluwer Academic Publishers, 1994. Part of the Water Science and Technology Library book series (WSTL, volume 13).
- W. Wada and M. Liou. *An accurate and robust flux splitting scheme for shock and contact discontinuities.* Siam Journal on Scientific Computing, 18, 05 1997. 10.1137/S1064827595287626
- K. Xu. *Gas evolution dynamics in godunov-type schemes and analysis of numerical shock instability.* Icase report no . 996. 1999.
- K. Xu and Z. Li. *Dissipative mechanism in godunov-type schemes.* International Journal for Numerical Methods in Fluids, 37:1–22, 09 2001. 10.1002/fld.160
- D. W.-M. Zaide. *Numerical Shockwave Anomalies* PhD Thesis, University of Michigan, 2012.
- D. Zaide and P. Roe. *Shock capturing anomalies and the jump conditions in one dimension.* 20th AIAA Computational Fluid Dynamics Conference 2011, 9126P–, 11 2011. 10.2514/6.2011-3686